Effect of wall corrugation on local convective heat transfer in coiled tubes

# Effect of wall corrugation on local convective heat transfer in coiled tubes

**Fabio Bozzoli[a,b], Luca Cattani[a], Sara Rainieri[a,b]**

[a] Department of Industrial Engineering, University of Parma,
Parco Area delle Scienze 181/A I-43124 Parma, Italy
[b] SITEIA.PARMA Interdepartmental Centre, University of Parma,
Parco Area delle Scienze 181/A, I-43124 Parma, Italy

E-mail address of the corresponding Author (Sara Rainieri): sara.rainieri@unipr.it

**Abstract**. The present paper presents the application of an inverse analysis approach to experimental infrared temperature data with the aim of estimating the local convective heat transfer coefficient for forced convection flow in coiled pipe having corrugated wall. The estimation procedure here adopted is based on the solution of the inverse heat conduction problem within the wall domain, by adopting the temperature distribution on the external coil wall as input data of the inverse problem: the unwanted noise is filtered out from the infrared temperature maps in order to make feasible the direct calculation of its Laplacian, embedded in the formulation of the inverse heat conduction problem, in which the convective heat transfer coefficient is regarded to be unknown. The results highlighted the local effects of both wall curvature and of wall corrugation on the convection heat transfer augmentation mechanism.

**Key words:** Compound heat transfer enhancement, Helically coiled tube, Corrugated tubes, Inverse Heat Conduction Problem.

## 1. Introduction

Among the most common passive techniques for enhancing convective heat transfer in ducts, rough surfaces, displaced enhancement devices, swirl-flow devices, curved geometries and flow additives are found [1-3]. These techniques are usually employed alone but it is well known that, in some cases, two or more of the existing techniques can be employed simultaneously to produce an enhancement larger than that produced by using only one technique. The combination of multiple techniques acting simultaneously is known as compound enhancement [2].

Different types of compound methods have been investigated in literature in order to verify in which conditions they are able to produce an enhancement larger than that produced by only one technique.

In [4-8] the passive compound heat transfer enhancement technique achievable by combining the effect of wall curvature and of wall corrugation was proved to be an interesting solution for optimizing the performance of helical-coiled heat exchangers for medium viscosity fluids.

The enhancement effect related to the helical coiling is due to the fact that the fluid experiences the centrifugal force that causes the fluid from the core region to be pushed towards the outer wall by producing a thinning of the boundary layers. Moreover, this phenomenon causes the generation of counter-rotating vortices that produce additional transport of fluid over the cross section of the pipe, by increasing heat transfer when compared to that found in a straight tube [9]. The enhancement effect associated to the wall corrugation is instead due to the periodic interruption of the boundary layers development, to the increase in heat transfer area, to the generation of swirling and/or secondary flows and to the promotion of the transition to an unstable regime [10].

The experimental data obtained by Rainieri et al. [4-6] showed that, for low Dean number values (*De* lower than about 120 for a corrugation depth and pitch of about 1 and 16 mm respectively) the wall curvature effect prevails and the heat transfer enhancement was the same for both the corrugated and the smooth helically coiled tube. On the contrary, for higher Dean number values, the wall corrugation brought an additional heat transfer enhancement. These outcomes highlight that the wall corrugated coils are a suitable tool to increase the overall thermal performances of the apparatuses employed in industrial applications where medium viscosity fluids are encountered, like in the food, chemical and pharmaceutics industries.

This compound enhancement techniques has been mainly discussed in the available scientific literature by considering only the heat transfer performance averaged over the tube perimeter and/or over the heat transfer surface area. This approximated approach, which is acceptable for many applicative cases, comes from the practical difficulty of measuring heat flux on the internal wall surface of a pipe. The size of the probes, the geometric inaccessibility of the surface, or a hostile environment prevent placing sensors on pipe internal wall. However, in some industrial applications, the knowledge of local thermal performances is of primary importance. For instance, in food pasteurisation, an excessively irregular temperature field could reduce the bacteria heat killing or locally overheat the product. Moreover, experimental data about the local convective heat transfer coefficient over the heat transfer surface could provide a deeper insight into the augmentation mechanisms for understanding the causal relationship between the heat transfer surface modification and the convection enhancement effect.

The present work aimed to start to fill this gap by presenting and testing an experimental procedure to estimate local heat-transfer coefficient in coiled tubes having corrugated wall. In order to single out the effect of wall curvature, also coiled tubes with smooth wall have been considered in the investigation.

The estimation procedure hereby presented is based on the solution of the Inverse Heat Conduction Problem (IHCP) within the wall domain by following a formulation that adopts the temperature distribution on the external coil wall as input data and in which the convective heat transfer coefficient distribution at the fluid-internal wall interface is regarded to be unknown [11]. Being the wall temperature distribution characterized by high spatial gradients, due to the complex effect of the wall corrugation on the flow pattern, the experimental methodology required a highly spatially resolved temperature measuring procedure, that was achieved by adopting a high precision cooled infrared camera. With this regard, it is worth remembering that the applications of thermographic systems to IHCPs are mainly limited to the use of focal plane array infrared cameras with cryogenic cooling, since they are characterized by a very good performance in terms of noise equivalent temperature difference [12-14].

As it is well known, IHCPs present some problems due to the fact that they are ill-posed showing a great sensitivity to variations in the input data such as the ones deriving from the experimental noise. In order to bypass these difficulties, that are particularly critical when infrared thermography is used as temperature measuring technique, many methods, based on the processing of experimental data, have been suggested and validated in literature. Among these techniques the conjugate gradient iterative method, the Laplace transform method, the sequential function specification method, the regularization methods such as Tikhonov regularization, the mollification method, the reciprocity function approach, the truncated singular value decomposition method and the filtering technique approach method are found [15-24].

Some of these techniques have been already successfully adopted to estimate local heat transfer coefficient in different pipe geometries [19,22,23,24] but they have never been applied to corrugated coils. For example, Lu et al. [25] implemented an estimation approach based on the IHCP solution, using the conjugate gradient method, to estimate the unknown transient fluid temperatures near the inner wall in section of a pipe elbow with thermal stratification. Su and Hewitt [26] estimated the time-dependent heat transfer coefficient of forced convective flow boiling over the outer surface of a heater tube solving an inverse heat conduction problem based on Alifanov's iterative regularization method. Rouizi et al. [27] employed the quadrupole method to retrieve the temperature and flux distributions over the internal surface of a micro-channel using temperature profiles measured at the external surface. Local convective heat transfer coefficient in coiled tubes was experimentally evaluated by Bozzoli et al. [24] using the Tikhonov regularisation method, the quadrupole method [19] and the filtering approach [23].

From the comparison of the different estimation approaches, it comes to light that the filtering approach is particularly suitable for problems with a high number of unknown variables and for input signal that are represented by spatially highly resolved temperature maps such as the infrared maps [28]. Moreover, this approach avoids the formulation of complex algorithms because the desired information (i.e., heat transfer coefficient or heat source distribution) can be derived by directly solving the heat conduction equation which uses as input data the denoised temperature field that is obtained by filtering the raw infrared maps.

In this paper the ill-conditioned nature of the IHCP was handled by applying the filtering technique on infrared temperature maps and this enabled to obtain the distribution of convective heat transfer coefficient in corrugated coils. Furthermore, the obtained results provided an improvement of the knowledge on this interesting compound convection enhancement technique highlighting the effect of wall curvature and of wall corrugation on the heat transfer augmentation mechanism.

## 2. Experimental facilities and image processing procedure

In the present investigation, a corrugated wall and a smooth wall helically coiled stainless steel type "AISI 304" tubes were tested. They both were characterized by eight coils with a helix diameter and a pitch of 310 mm and 200 mm, respectively, thus yielding a coiled pipes length $L$ of approximately 10 m. The corrugated-wall tube considered in the present investigation is included in the general category usually known as spirally enhanced tubes, exemplified in Fig.1. It presented an internal helical ridging corresponding to an external helical grooving, obtained by embossing a smooth stainless steel tube. In particular, the tube under test had a wall thickness of 1 mm and an external envelope radius $r_{ext}$ of 8 mm, while the corrugation profile had a depth $e$ of 1 mm and a pitch $p$ of 16 mm.

The working fluid was carried to a holding tank using a volumetric pump and entered the coiled test section equipped with stainless-steel fin electrodes, which were connected to a power supply of the type HP 6671A. This setup allowed the investigation of the heat transfer performance of the tube under the prescribed condition of uniform heat generation in the wall by Joule effect. The coiled section was inserted horizontally in a loop, which was completed with a secondary heat exchanger, fed with city water to maintain a constant working fluid temperature at the tube inlet.

The heat flux provided to the fluid was selected to make the buoyancy forces negligible in comparison to inertial ones for the investigated fluid velocity ranges.

To minimize the heat exchange to the environment, the heated section was thermally insulated using a cellular rubber layer, which was 40 mm thick. A small portion of the external tube wall was made accessible to a thermal imaging camera by removing the thermally insulating layer, and the wall portion was coated with a thin film of high emissivity paint. This thin paint layer changes the surface emissivity without affecting the heat conduction problem in the tube wall.

The surface temperature distribution was obtained using a FLIR SC7000 infrared camera with a 640 x 512 pixel sensor. As reported by the instrument manufacturer, its thermal sensitivity is 20 mK at 303 K, and its accuracy is ±1 K. A schematic view of the experimental setup and of the infrared thermographic system arrangement are shown respectively in Figs. 2a-b.

The inlet fluid bulk temperature was measured through a type-T thermocouple, which was previously calibrated and connected to a multichannel ice point reference of type KAYE K170-50C. The bulk temperature at any location in the heat transfer section was calculated from the net power supplied to the tube wall [24,29]. The volumetric flow rate was obtained by measuring the required time to fill a volumetric flask at the outlet of the test section.

Ethylene Glycol was used as the working fluid with the aim of investigating specific Reynolds and Dean numbers values for which different flow regimes are expected to establish as a consequence of both the wall curvature and the wall corrugation effect. In the temperature range of the experimental conditions, the

Prandtl number of the working fluid varied in the range of 170 to 200, whereas the wall-to-bulk-fluid temperature difference was limited within 10 K. Therefore, the fluid property variation effect through the thermal boundary layer was considered negligible.

In the present experimental investigation, the fully developed thermal condition was considered. Therefore, the test section was taken near the end of the heated section, where both hydrodynamic and thermal boundary layers reached the asymptotic profile [30].

To measure the temperature distribution on the whole test section surface, multiple images were acquired, moving the infrared camera around the tube's axis. A representative infrared image is reported in Fig. 3.The effective emissivity of the surface was estimated in situ by shooting a target at different known temperatures [14,31,32], and the value 0.99 was found. The acquired images, thanks to adequate position references fixed on the tube wall, were conveniently processed to obtain continuous temperature map on the tube wall.

The image processing procedure was made complex by the fact that the observed target surface is not flat: common photo-plans can be produced from images of planar objects by image processing tools based on well-known equations of central projection but this is not really an easy task when dealing with curved objects [33]. The image processing procedure adopted in this paper permits to rectify optical deformations of the collected images caused by surface curvature. This procedure assumes that the coil portion viewed by the infrared camera could be modeled as a cylindrical surface, an assumption that is acceptable since the helix diameter is significantly bigger than tube external diameter and the distortion effect produced on the pipe external surface by the corrugation is minimal. Fig. 4 sketches how a cylindrical surface is projected on a plane when the plane is parallel to the cylinder axis.

Under the assumption that the camera is sufficiently far from the pipe, from (x,y), which are the coordinates of an image point in the plane reference system, the corresponding coordinates (α, z) in the cylindrical coordinate system can be calculated as follows:

$$\begin{cases} z = \Omega \cdot y + z_0 \\ \alpha = \arctan(x/\Psi) + \alpha_0 \end{cases} \quad (1)$$

where $\Psi$, $\Omega$, $z_0$ and $\alpha_0$ are parameters, depending on camera lenses and camera relative position. These parameters can be easily determined by calibrating the acquisition system with a known sample pattern fixed on the tube wall [33,34].

In order to validate this surface reconstruction algorithm, the typical “chessboard test” was performed: the pattern shown in Fig. 5 was glued on the tube external surface and shot by a digital camera. The obtained pictures were elaborated by the above described procedure that is usually called “texture unwrapping”.

In Fig. 6 the processing steps of a sample image are reported. It is easy to notice from Fig. 6b that, for clear geometrical causes, the unwrapping of the image close to the pipe borders is not perfectly achievable and for this reason only the central part of the processed image was considered in the surface reconstruction process.

In order to reconstruct the whole image of the test surface, the camera was moved around the section acquiring 7 different images that were then unwrapped with the procedure discussed above; finally, thanks to the position references (i.e. letters above and below the chessboard pattern) the unwrapped images were merged together to obtain the continuous map on the tube wall (Fig. 7). The comparison between the final unwrapped image (Fig. 7) and the original source pattern (Fig. 5) confirms the effectiveness of the procedure.

This procedure was applied to infrared images to obtain continuous temperature map on the tube wall: in Fig. 8 a representative unwrapped infrared image is reported.

## 3. Parameter estimation procedure

To evaluate the local actual value of the convective heat transfer coefficient at the fluid internal wall interface on a given cross section, the following procedure was followed: the temperature distribution was acquired on the external wall surface of a given test section in which the internal heat generation source was provided by the Joule effect; then, the IHCP in the wall domain was solved by considering that the convective heat transfer coefficient distribution on the internal wall surface was unknown.

The physical problem is represented by the heat conduction in the wall of a corrugated pipe (see Fig.1) and in this domain the steady state energy balance equation is expressed in the form:

$$k\nabla^2 T + q_g = 0 \qquad (2)$$

where $q_g$ is the heat generated per unit volume within the tube wall having thermal conductivity $k$.

The energy balance equation is completed by the following two boundary conditions:

$$-k\nabla T = \frac{(T - T_{env})}{R_{env}} \tag{3}$$

that is applied on the external surface of the cylindrical shell and where $R_{env}$ is the overall heat transfer resistance between the tube wall and the surrounding environment with the temperature $T_{env}$ ,

$$-k\nabla T = -h_{\mathrm{int}}(T - T_b) \tag{4}$$

that is applied on the internal surface of the cylindrical shell and where $T_b$ is the fluid local bulk temperature. In order to implement the parameter estimation procedure proposed in this paper a simplified numerical model of the test section (sketched in Fig. 9) was considered: it was formulated by assuming that the coil portion viewed by the infrared camera could be modeled as a finite section of a circular cylindrical shell. This model introduced a negligible error, since the helix diameter is significantly bigger than tube external diameter and wall corrugation, when present, didn't significantly modify the thickness of the tube wall.

By assuming the thin-wall approximation, the temperature on the external surface was considered equal to that on the internal surface:

$$T(\alpha, r, z) \cong T(\alpha, r_{\mathrm{int}}, z) \cong T(\alpha, r_{ext}, z) \tag{5}$$

The thin-wall approximation is acceptable when the Biot number, that is defined as the convective heat transfer coefficient multiplied by the tube thickness and divided by the tube thermal conductivity, is smaller than 0.1 , [35]. This condition was verified for the cases under study.

With reference to the infinitesimal cylindrical sector as described in Fig. 10, the steady state local energy balance equation becomes:

$$Q_{\alpha+d\alpha} + Q_{\alpha} + Q_{r_{\mathrm{int}}} + Q_{r_{ext}} + Q_z + Q_{z+dz} + Q_g = 0 \tag{6}$$

The heat flux along the angular coordinate $\alpha$ is expressed as follows:

$$Q_{\alpha} = \int_{r_{\mathrm{int}}}^{r_{ext}} -\frac{k\partial T}{r\partial\alpha} drdz = -\frac{kdT}{d\alpha}\ln\left(\frac{r_{ext}}{r_{\mathrm{int}}}\right)dz \tag{7}$$

$$Q_{\alpha+d\alpha}=-\left(Q_{\alpha}+\frac{\partial Q_{\alpha}}{\partial\alpha}d\alpha\right)=-\left[-k\frac{\partial T}{\partial\alpha}\ln\left(\frac{r_{ext}}{r_{\mathrm{int}}}\right)dz+\frac{\partial}{\partial\alpha}\left(-k\frac{\partial T}{\partial\alpha}\ln\left(\frac{r_{ext}}{r_{\mathrm{int}}}\right)dz\right)d\alpha\right]=$$
$$=k\frac{\partial T}{\partial\alpha}\ln\left(\frac{r_{ext}}{r_{\mathrm{int}}}\right)dz+k\frac{\partial^2 T}{\partial\alpha^2}\ln\left(\frac{r_{ext}}{r_{\mathrm{int}}}\right)d\alpha dz \tag{8}$$

where $r_{int}$ and $r_{ext}$ are the internal and the external pipe radius, respectively.

In Eqs. (9-10) the contributions along the radial coordinate $r$ are defined:

$$Q_{r_{\mathrm{int}}}=-h_{\mathrm{int}}(T-T_b)r_{\mathrm{int}}d\alpha\,dz \tag{9}$$

$$Q_{r_{ext}}=-\frac{(T-T_{env})}{R_{env}}r_{ext}d\alpha dz \tag{10}$$

The axial components of the heat flux are expressed in Eqs. (11-12):

$$Q_z=\int_{r_{\mathrm{int}}}^{r_{ext}}-k\frac{\partial T}{\partial z}\frac{\pi r^2}{2\pi}d\alpha dr=-k\frac{\partial T}{\partial z}\frac{(r_{ext}^2-r_{\mathrm{int}}^2)}{2}d\alpha \tag{11}$$

$$Q_{z+dz}=-\left(Q_z+\frac{\partial Q_z}{\partial z}dz\right)=-\left[-k\frac{\partial T}{\partial z}\frac{(r_{ext}^2-r_{\mathrm{int}}^2)}{2}d\alpha+\frac{\partial}{\partial z}\left(-k\frac{\partial T}{\partial z}\frac{(r_{ext}^2-r_{\mathrm{int}}^2)}{2}d\alpha\right)dz\right]=$$
$$=k\frac{\partial T}{\partial z}\frac{(r_{ext}^2-r_{\mathrm{int}}^2)}{2}d\alpha+k\frac{\partial^2 T}{\partial z^2}\frac{(r_{ext}^2-r_{\mathrm{int}}^2)}{2}d\alpha dz \tag{12}$$

Finally the heat source term is defined as:

$$Q_g=q_g\frac{(\pi r_{ext}^2-\pi r_{\mathrm{int}}^2)}{2\pi}d\alpha dz=\frac{q_g}{2}\cdot(r_{ext}^2-r_{\mathrm{int}}^2)d\alpha dz \tag{13}$$

Substituting Eqs. (7-13) into Eq. (6) the energy equation becomes:

$$h_{\mathrm{int}}\cdot r_{\mathrm{int}}\cdot(T-T_b)-k\cdot\ln\left(\frac{r_{ext}}{r_{\mathrm{int}}}\right)\cdot\frac{\partial^2 T}{\partial\alpha^2}-\frac{k}{2}(r_{ext}^2-r_{\mathrm{int}}^2)\cdot\frac{\partial^2 T}{\partial z^2}+\frac{r_{ext}}{R_{env}}(T-T_{env})-\frac{q_g}{2}(r_{ext}^2-r_{\mathrm{int}}^2)=0 \tag{14}$$

Eventually, the convective heat transfer coefficient on the internal wall surface follows as:

$$h_{\mathrm{int}}=\frac{k\cdot\ln\left(\frac{r_{ext}}{r_{\mathrm{int}}}\right)\cdot\frac{\partial^2 T}{\partial\alpha^2}+\frac{k}{2}(r_{ext}^2-r_{\mathrm{int}}^2)\cdot\frac{\partial^2 T}{\partial z^2}-\frac{r_{ext}}{R_{env}}(T-T_{env})+\frac{q_g}{2}(r_{ext}^2-r_{\mathrm{int}}^2)}{r_{\mathrm{int}}\cdot(T-T_b)} \tag{15}$$

This equation, if applied to discrete noisy data, gives unreliable results due to the peculiarities of the second derivative operator that is very sensitive to small perturbations in the input data due to the well-known destructive effect of the noise [11]. A convenient way to overcome these difficulties is found in filtering out the unwanted noise from the raw temperature data in order to make feasible the direct calculation of its Laplacian. The effectiveness of the Gaussian kernel in this kind of approach was experimented by Murio et al. [18], Delpueyo et al. [21] and Bozzoli et al. [14, 20].

The application of a Gaussian filter has the effect of reducing the data high-frequency components and it behaves then in a way similar to a regularization function. It is widely adopted in the enhancing of images' quality within graphics software. The transfer function in a 2-D frequency domain, of this kind of filter can be expressed as follows:

$$H(u,v) = e^{-\left(u^2+v^2\right)/2u_c^2} \tag{16}$$

where $u_c$ is the cutoff frequency, assumed equal along the $u$ and $v$ coordinates. Since in real applications the optimal cutoff frequency value for each kind of filter is not known a priori, a criterion to choose it must be selected in order to make successful the regularization procedure. This choice is similar to the selection of optimal regularization parameters when dealing with regularization methods for inverse estimation [11]. In the present analysis the criterion provided by the discrepancy principle, originally formulated by Morozov [36], was adopted.

According to this principle, the inverse problem solution was regarded to be sufficiently accurate when the difference between measured temperatures $\boldsymbol{Y}$ and filtered ones $\boldsymbol{Y}_f$ was close to the standard deviation of the raw measurements. The cutoff frequency was then determined as the frequency at which the following condition was satisfied:

$$\frac{\left\| Y_f - Y \right\|_2^2}{N \cdot M} = \sigma_Y{}^2 \tag{17}$$

where $\|\;\|_2$ stands for the 2-norm, $N{\cdot}M$ is the size of the matrix $\boldsymbol{Y}$ and $\sigma_Y$ is the standard deviation of the noise, that was estimated by measuring the surface temperature distribution while maintaining the coil wall under isothermal conditions. In other words, the discrepancy principle tailors the filter according to the noise level, which implies that the best expected approximation is in the order of the data random error that affect the measurements [36].

## 4. Validation of the estimation procedure

To validate the procedure presented above, synthetic temperature data were generated by solving the direct problem with a known distribution of convective heat transfer coefficient $h_{int}$ at the internal wall surface. The numerical model, implemented within Comsol Multiphysics ® environment, considered a finite section of a corrugated coil.

According to what is expected to find in the real case, as convective heat transfer coefficient $h_{int}$ it was considered a distribution characterized by a significant variation both along the circumferential and the axial coordinate:

$$h_{int} = A + B \cdot \sin\left(\alpha + 2\pi \cdot (z/p)\right) \tag{18}$$

where $p$ was taken equal to corrugation pitch and $A$ and $B$ as representative values were chosen to be equal respectively to 400 $W/m^2K$ and 300$W/m^2K$.

The solution of the direct heat conduction problem within the solid wall according to the parameter reported in Table 1, enabled to find a synthetic temperature distribution on the external wall surface. This temperature distribution, spoiled by random noise, was then used as the input data of the inverse problem. Fig. 12 shows a representative noisy temperature distribution. In particular, a Gaussian noise characterized by a standard deviation ranging from 0.01 K – 1 K was employed.

In Fig. 13 the heat transfer coefficient distribution, obtained by applying the filtering technique, presented in Section 3, on the representative case of noisy data of Fig. 12 is reported. The reconstructed values are compared with the original local heat transfer distribution in Figs. 14a-b referring to the circumferential distribution (at z=0.008 m) and to the axial distribution (at α=0 rad). From these comparisons, it is clear that the reconstructed values match with a good approximation the original local convective heat transfer distribution although there is a not negligible smoothing in correspondence of the peaks, typical of filtering approach [20,28].

In order to quantify the effectiveness of the approach at different signal to noise ratio values, residual analysis was performed by plotting in Fig. 15 the estimation error, defined as follows:

$$E_h = \frac{\left\| (h_{\text{int}})_{restored} - (h_{\text{int}})_{exact} \right\|_2}{\left\| (h_{\text{int}})_{exact} \right\|_2} \tag{19}$$

versus the standard deviation present in the input data.

These results highlight that, for the problem here investigated, the Gaussian filter approach performs efficiently until the values of about σ = 0.2 K presenting a value of $E_h$ lower than 10%. After that value, the estimation error grows steeply with the increasing of the noise level. It has to be noted that the estimation error isn't negligible also for very small levels of noise (i.e., it is 5% for σ = 0.01 K) and it is related to the thin wall approximation which is present in the estimation procedure.

## 5. Results and discussion

### *5.1 Experimental data*

The experimental conditions were designed in order to single out the effect of both wall curvature and of wall corrugation. Therefore different Dean number values, representative of two flow regimes in which the effect of the corrugation was expected to be significantly different, were considered. The Dean number was defined as follows:

$$De = \frac{2\,w \cdot r_{\text{int}}}{\nu_f}\sqrt{\frac{2\,r_{\text{int}}}{a}} \tag{20}$$

where $w$ is the mean fluid axial velocity, $r_{int}$ is the maximum tube internal diameter, $a$ is the coil diameter and $\nu_f$ is the fluid kinematic viscosity, evaluated at the local bulk fluid temperature.

In particular Dean number values lower than 120 and greater than 120 were considered; in fact the value 120 was verified by Rainieri et al. [6] as the critical value for a similar corrugation profile that suitably describes the departure from a flow regime where the wall curvature effect prevails towards a different flow regime in which the wall corrugation is able to bring an additional enhancement effect.

The convective heat transfer coefficient can be also expressed in a dimensionless form by means of the Nusselt number, as follows:

$$Nu = \frac{h_{\text{int}} \cdot D_{\text{int}}}{k_f} \tag{21}$$

where $k_f$ is the fluid thermal conductivity, evaluated at the bulk temperature

The asymptotic Nusselt number for the two tube geometries considered in this paper was measured in [6] and was reported in Fig. 16 vs. the Dean number and compared to the performance of the straight tube with smooth wall [35]. These data highlight that both wall curvature and wall corrugation are responsible for an additional convective transport mechanism that increases the heat transfer when compared to that in a straight tube. The effect of the wall curvature alone brings heat transfer enhancement in the range 200% ÷ 1000% , while for the helical coiled corrugated tubes an heat transfer augmentation up to 2500% was registered.

The wall temperature maps, as reconstructed by the unwrapping algorithm described in Section 2, are reported in Fig. 17 for the different Dean number values. In the representation, the outer side of the coil correspond to the angular coordinate value of 1.9 rad and the inner side to the value of 5.0 rad. Fig. 18 reports the position of the corrugation on the tube surface. In Fig. 18 also the wall temperature maps for the smooth wall coiled tube are reported for similar Dean number values. The details of the experimental conditions are reported in Table 2.

The data show that for both the smooth-wall and the corrugated-wall pipe, the wall temperature distribution for the lowest *De* values exhibits a significant variation along the circumference and this is necessarily to be ascribed to the onset of the Dean vortices due to coiled shape of the pipe, while the temperature gradient is almost negligible along the axis of the tube, as it was observed for coiled tubes with smooth wall by Bozzoli et al. [24]. In particular, under heating condition, the fluid layer is significantly colder at the coil outside while it is hotter at the coil inside, due to the secondary flow pattern induced by the centrifugal force.

For the highest Dean number values, the temperature distribution profile keeps almost unchanged for the smooth-wall coiled tube. On the contrary, in this flow regime, the temperature distribution measured on the external wall surface of the corrugated helically coiled tube, shows a significant deformation that clearly resembled the corrugation profile and it can be noticed by comparing Fig. 17 to Fig. 18. In this condition the temperature gradient along the tube axis, induced by the complex flow pattern, couldn't be neglected. From the two intermediate values it is possible to follow the evolution of the transition between the two flow regimes: for *De* = 78 is already possible to observe the onset of the effect of the corrugation that modifies the temperature distribution introducing also an axial gradient and with the increasing of Dean number values (see for instance *De* = 156) this phenomenon becomes more and more consistent.

To better single out the effect of both wall curvature and of wall corrugation that acts on the circumferential and axial distributions of the temperature, the circumferential distributions are reported in Fig. 19 for different values of the axial coordinate z . These plots confirm that for the lowest *De* values, for both the smooth wall and the corrugated wall pipe, there are significant temperature variations along the circumference, due to the distortion of the velocity profile caused by the centrifugal force. The differences between the smooth wall coil and the corrugated ones starts to be noticeable for higher Dean number values: for the two highest Dean number values the distortion of the temperature profile due to the presence of the corrugation becomes more important.

### *5.2 Sensitivity and Uncertainty analysis*

The infrared temperature maps were processed by the filtering technique in order to restore the convective heat transfer coefficient distribution by solving Eqs. (6-15). The overall heat transfer resistance between the tube wall and the surrounding environment $R_{env}$ was taken equal to 0.2 $m^2K/W$, that is a representative value for natural convection in air compounded with radiative heat transfer with the environment; for the wall thermal conductivity $k$ the value 15 W/mK was assumed as certified by the manufacturer; the heat generated by the Joule effect in the wall $q_g$ was calculated by the ratio of the power supplied and the volume of the tube wall; the temperature uncertainty was estimated by measuring the surface temperature distribution while maintaining the coil wall under isothermal conditions. The uncertainty assumed in the input data are reported in Table 3.

To identify the main contributions to the uncertainty of the estimated heat flux distribution a sensitivity analysis and the calculation of the influence coefficient values [37] were performed:

$$J_{\xi}^{Z} = \left( \frac{\partial Z}{\partial \xi} w_{\xi} \right)^{2} \qquad (22)$$

where $Z$ is the estimated quantity and $\xi$ is the considered input parameter with an uncertainty equal to $w_{\xi}$. For the problem here investigated , the analytical determination of the sensitivity $\partial Z/\partial \xi$ was not feasible, and finite difference approach was adopted.

The computed sensitivities for the main input parameters for a significant case (i.e., corrugated wall tube for Re=733) , are reported in Table 4. The maximum and the minimum of the estimated convective heat transfer coefficient has been considered as representative output quantities of the inverse problem solution. The corresponding influence parameters for the same input quantities are reported in Table 5. From these results it is possible to notice that the main contributions to the uncertainty are the $k$, $q_g$ and $T_b$ measurements while the uncertainties on $R_{env}$ and $T_{env}$ are not very significant. From this observation it is possible to state that the heat exchanged between the tube wall and the environment is negligible in comparison to the heat exchanged between the tube wall and the working fluid and that particular attention to the accuracy of $k$, $q_g$ and $T_b$ should be given.

The uncertainty analysis was performed by using the well known propagation of errors procedure [38] considering the uncertainty on the input parameters assumed in Table 3 and the results of the validation process presented above, yielding an overall uncertainty on the local value of $h_{int}$ of about 12 %.

### *5.3 Convective heat transfer coefficient estimation*

The restored convective heat transfer coefficient distribution are reported in Fig. 20 for the eight cases above considered.

Before analyzing the local convective heat transfer distributions, it is convenient remembering that, as observed in Fig. 16 for the asymptotic Nusselt number, for low Dean number values the heat transfer performance of the corrugated and smooth wall tubes are equivalent: thus the main effect that promotes the heat transfer enhancement is the centrifugal force experienced by the fluid due to the coiled shape of the pipe that produces a thinning of the boundary layers and the generation of counter rotating vortices. Then for higher Dean number values the heat transfer enhancement obtainable by adopting the corrugated wall pipes is more than the one achievable by smooth wall coiled tubes: this increase is due to the fact that to the phenomenon induced by the centrifugal force is added the periodic interruption of the boundary layers development produced by the wall corrugation.

The distributions reported in Fig. 20 confirm that for lowest *De* value the wall curvature effect prevails and the presence of the corrugation does not strongly impact on the convective heat-transfer coefficient distributions. In this flow regime the convective heat transfer coefficient is significantly higher at the coil outside with respect to the coil inside, as reported by other Authors [39-41]. In particular at the outside surface of the coil, $h_{int}$ is approximately five times than that at the inside surface, while it doesn't show significant variation along the tube axis. For the highest De values instead, the wall corrugation significantly affects the fluid flow, by bringing a further heat transfer enhancement. For *De*=207 the convective heat-transfer coefficient distribution is strongly irregular with respect to the one of the smooth wall pipe (*De*=215) that remains similar to the case of low *De*: in particular the comparison of Fig. 20$d_1$ with Fig. 18 highlights that the distribution in the corrugated coil has a local maximum and a local minimum close to the crest and downstream of the corrugation, respectively. This behavior can be ascribed to the boundary layers disruption effect due to surface roughness encountered by the fluid along its path and to the recirculation zone occurring downstream of the corrugation.

From Fig. 21, where the circumferential $h_{int}$ distributions for the four Dean numbers at different *z* positions are reported, it is possible to notice that for *De*=33 the heat transfer coefficient distributions for the corrugated wall tube clearly show the effect of the Dean vortices while the profile doesn't change significantly along the tube axis and the effect of the wall corrugation is almost negligible as it happens for the smooth wall pipe (*De*=29). For the highest Dean number values (*De*=207) instead the effect of the wall roughness becomes important and the convective heat transfer coefficient distribution changes significantly along the tube axis when the fluid crosses the corrugation profile.

The results have been reported in terms of local convective heat transfer coefficient $h_{int}$ but all the parameters needed to compute the Nusselt number are reported in Table 2.

In addition in Fig. 22 the $h_{int}/h_{int,max}$ ratio distributions for the two extreme Dean numbers at different *z* positions are reported for both the smooth and corrugated wall pipes and compared to the best fit of a set of experimental distributions (25 < *De* < 240) obtained for a similar smooth wall coiled tube by Bozzoli et al. [24]. These local data clarify the results of Rainieri et al. [6]: for coiled tubes with corrugated wall, a critical

Dean number exists above which the wall corrugation, as superimposed to the wall curvature, brings an additional heat transfer enhancement. For high Dean number values the augmentation phenomenon induced by the periodic interruption of the boundary layers development produced by the wall corrugation is added to the effects of the centrifugal force. Moreover, the $h_{int}/h_{int,max}$ ratio distributions highlight that, although compound effect of wall curvature and of wall corrugation ends in an overall heat transfer enhancement as compared to the smooth wall coiled tube, a drawback of this enhancement arises since an important irregular distribution of the convective heat transfer coefficient is observed; in the smooth wall coils the minimum value of $h_{int}/h_{int,max}$ is about 0.2 while in corrugated wall coils it is around 0.1. This behavior could affect the performances of many industrial processes and has to be taken into serious account in the design of industrial apparatus based on this geometrical configuration.

**5. Conclusions**

The present paper presents the application of an inverse analysis approach to experimental infrared temperature data aimed to estimate the local convective heat transfer coefficient for forced convection flow in coiled pipe having smooth and corrugated wall. The estimation procedure is based on the filtering approach applied to the solution of the inverse heat conduction problem within the wall domain. The unwanted noise is filtered out from the infrared temperature maps acquired on the external pipe wall in order to make feasible the direct calculation of its Laplacian, embedded in the formulation of the inverse heat conduction problem in which the convective heat transfer coefficient is regarded to be unknown. The results obtained highlight the effect of both wall curvature and of wall corrugation on the convection heat transfer augmentation mechanism.

These local experimental heat transfer coefficient distributions show that, for coiled tubes with corrugated wall, a critical Dean number exists above which the wall corrugation, as superimposed to the wall curvature, brings an additional heat transfer enhancement. For low values of Dean number the convective heat transfer coefficient distributions obtained for smooth and corrugated wall are comparable confirming that for this regime the increasing effects has to be ascribed to the wall curvature. While, for high *De* values the corrugation effect start to prevail producing a significant enhancement of the heat transfer. However, the drawback of this enhancement is a more irregular distribution of the convective heat transfer coefficient, compared to the smooth wall coil.

These results are representative of a wide range of technical applications and they might be particularly useful in the validation of numerical models or in the design of innovative coiled tube heat exchangers.

## NOMENCLATURE

| Symbol | Quantity | SI Unit |
|---|---|---|
| $a$ | Coil diameter | m |
| $c_p$ | Specific heat at costant pressure | J/kg·K |
| $e$ | Wall thickness | m |
| $De$ | Dean number | |
| $h$ | Convective heat-transfer coefficient | $W/m^2 \cdot K$ |
| $k$ | Thermal conductivity | W/mK |
| $p$ | Coil pitch | m |
| $q$ | Convective heat flux per unit area | $W/m^2$ |
| $r$ | Radial coordinate | m |
| $Re$ | Reynolds number | - |
| $T$ | Temperature | K |
| $u,v$ | Frequency components | $rad^{-1}$ |
| $u_c$ | Cutoff frequency | $rad^{-1}$ |
| $z$ | Axial coordinate | m |
| $w$ | Mean fluid axial velocity | m/s |
| $H$ | Transfer function | |
| $J$ | Influence coefficient | |
| $Q$ | Convective Heat flux | W |
| $Q_g$ | Internal heat generation | W |

| | | |
|---|---|---|
| $R_{env}$ | Overall heat-transfer resistance between the external tube wall and the surrounding environment | $m^2 \cdot K / W$ |
| $Nu$ | Nusselt number | |
| $Y$ | Measured temperature | K |
| $\alpha$ | Angular coordinate | rad |
| $\mu$ | Dinamic viscosity | Pa·s |
| $\nu$ | Kinematic viscosity | $m^2/s$ |

*Subscripts,superscripts*

| | |
|---|---|
| *b* | Bulk |
| *env* | Environment |
| *ext* | External |
| *f* | Fluid |
| *int* | Internal |

**Acknowledgments**

This work was partially supported by Emilia-Romagna Region (POR FSE 2007-2013).

MBS srl is gratefully acknowledged for the set-up of the experimental apparatus. The Authors thank Mr. Michele Rossi for the help in the experimental activity.

**References**

[1] Webb R., Kim H.H., Principles of Enhanced Heat Transfer, 2nd ed., New York: Taylor & Francis 2005.

[2] Bergles A.E., Techniques to enhance heat transfer in: Handbook of Heat Transfer, New York: McGraw-Hill, 1998.

[3] T. Kuppan, Heat Exchanger Design Handbook, New York: Marcel Dekker Inc., 2000.

[4] Rainieri S., Bozzoli F., Pagliarini G., Experimental Investigation on the Convective Heat Transfer in Straight and Coiled Corrugated Tubes for Highly Viscous Fluids: Preliminary Results, International Journal of Heat and Mass Transfer 7(55) (2012) 498- 504.

[5] Rainieri S., Bozzoli F., Cattani L., Pagliarini G., Experimental investigation on the convective heat transfer enhancement for highly viscous fluids in helical coiled corrugated tubes, Journal of Physics: Conference Series 395 (1) (2012) Article number 012032.

[6] Rainieri S., Bozzoli F., Cattani L., Pagliarini G., Compound convective heat transfer enhancement in helically coiled wall corrugated tubes, International Journal of Heat and Mass Transfer 10(59) (2013) 353-362.

[7] Zachár A., Analysis of coiled-tube heat exchangers to improve heat transfer rate with spirally corrugated wall, International Journal of Heat and Mass Transfer 53(19) (2010) 3928–3939.

[8] Li Y.x., Wu J.H., Wang H,. Kou L.P.,. Tian X.H., Fluid flow and heat transfer characteristics in helical tubes cooperating with spiral corrugation, Energy Procedia 17 (2012) 791–800.

[9] Naphon P., Wongwises S., A review of flow and heat transfer characteristics in curved tubes, Renewable & Sustainable Energy Reviews 10 (2006) 463–490.

[10] Rozzi S., Massini R., Paciello G., Pagliarini G., Rainieri S., Trifirò A., Heat treatment of fluid foods in a shell and tube heat exchanger: comparison between smooth and helically corrugated wall tubes Journal of Food Engineering 79(1) 2007 249–254.

[11] Beck J.V., Balckwell B., St. Clair Jr C.R., Inverse Heat Conduction – Ill-posed problems, New York: John Wiley & Sons Inc. 1985.

[12] Rogalski A., Optical detectors for focal plane arrays, Optical detectors for focal plane arrays, Opto-Electronics Review 12(2) (2004) 221–245.

[13] Rogalski A., Recent progress in infrared detector technologies, Infrared Physics & Technology 54 (3) (2011) 136-154.

[14] Rainieri S., Bozzoli F., Pagliarini G., Characterization of an uncooled infrared thermographic system suitable for the solution of the 2-D inverse heat conduction problem, Experimental Thermal and Fluid Science 32(8) (2008), 1492-1498.

[15] Orlande H.R.B., Fudym O., Maillet D., Thermal Measurements and Inverse Techniques, Boca Raton: CRC Press, Taylor & Francis Group, 2011.

[16] Özisik M.N., Orlande H.R.B., Inverse Heat Transfer, New York: Taylor & Francis, 2000.

[17] Renault N., André S., Maillet D., Cunat C., A two-step regularized inverse solution for 2-D heat source reconstruction, International Journal of Thermal Sciences 47 (2008) 834–847.

[18] Murio A.D., The Mollification Method and the Numerical Solution of Ill-Posed Problems, New York: John Wiley and Sons 1993.

[19] Cattani L., Maillet D., Bozzoli F., Rainieri S., Estimation of the local convective heat transfer coefficient in pipe flow using a 2D thermal Quadrupole model and Truncated Singular Value Decomposition, International Journal of Heat and Mass Transfer 91 (2015) 1034-1045.

[20] Bozzoli F., Pagliarini G., Rainieri S., Experimental validation of the filtering technique approach applied to the restoration of the heat source field, Experimental Thermal and Fluid Science 44 (2013) 858-867.

[21] Delpueyo D., Balandraud X., Grédiac M., Heat source reconstruction from noisy temperature fields using an optimised derivative Gaussian filter, Infrared Physics & Technology 60 (2013) 312–322.

[22] Colaço M.J., Alves C.J.S., Bozzoli F., The reciprocity function approach applied to the non-intrusive estimation of spatially varying internal heat transfer coefficients in ducts: Numerical and experimental results, International Journal of Heat and Mass Transfer 90 (2015) 1221-1231.

[23] Bozzoli F., Cattani L., Pagliarini G., Rainieri S., Infrared image filtering applied to the restoration of the convective heat transfer coefficient distribution in coiled tubes, Opto-Electronics Review 23 (1) (2015) 109–117.

[24] Bozzoli F., Cattani L., Rainieri S., Bazán F.S.V., Borges L.S., Estimation of the local heat-transfer coefficient in the laminar flow regime in coiled tubes by the Tikhonov regularisation method, International Journal of Heat and Mass Transfer 72 (2014) 352-361.

[25] Lu T., Liu B., Jiang P.X., Zhang Y.W., Li H., A two-dimensional inverse heat conduction

problem in estimating the fluid temperature in a pipeline, Applied Thermal Engineering 30 (2010) 1574-1579.

[26] Su J., Hewitt G.F., Inverse heat conduction problem of estimating time-varying heat transfer coefficient, Numerical Heat Transfer 45 (2004) 777-789.

[27] Rouizi Y., Maillet D., Jannot Y., Fluid temperature distribution inside a flat mini-channel: semi-analytical wall transfer functions and estimation from temperatures of external faces, International Journal of Heat and Mass Transfer 64 (2013) 331-342.

[28] Carlomagno G.M., Cardone G., Infrared thermography for convective heat transfer measurements, Experiments in Fluids 49 (6) (2010) 1187–1218.

[29] Bozzoli F., Cattani L., Rainieri S., Pagliarini G., Estimation of the local heat transfer coefficient in coiled tubes under heat conduction problem approach, Experimental Thermal and Fluid Science, 59 (2014) 246-251.

[30] Janssen L.A.M, Hoogendoorn C.J., Laminar convective heat transfer in helical coiled tubes, International Journal of Heat and Mass Transfer 21 **(**1978**)** 1197–1206.

[31] Xu J.L., Shen S., Gan Y.H., Li Y.X., Zhang W., Su Q.C., Transient flow pattern based microscale boiling heat transfer mechanisms, Journal of Micromechanics and Microengineering 15 (6) (2005) 1344-1361.

[32] Xu J.L., Gan Y.H., Zhang D.C., Li X.H., Microscale heat transfer enhancement using thermal boundary layer redeveloping concept, International Journal of Heat and Mass Transfer 48(9) (2005) 1662-1674.

[33] Pavelka K., Ruzicka S., Bila Z., Photo-plan creation of cylindrical objects, ISPRS Annals of the Photogrammetry, Remote Sensing and Spatial Information Sciences, Volume II-5/W1, 2013.

[34] Cyganek B., Siebert J.P., An Introduction to 3D Computer Vision Techniques and Algorithms, New York: Wiley 2011.

[35] Incoprera F.P., De Witt D.P., Fundamentals of Heat and Mass Transfer, John Wiley & Sons, Inc New York (2002).

[36] Morozov V.A., Methods for Solving Incorrectly Posed Problems, New York: Springer-Verlag

1984.

[37] Holman J.P., Experimental Methods for Engineers-7/E, McGraw_Hill (2001).

[38] Kline S.J. and McClintock, Describing uncertainties in single –sample experiments, Mechanical Engineering (1953).

[39] Ravigururajan T.S., Bergles A.E., Visualization of Flow Phenomena near Enhanced Surfaces, Journal of Heat Transfer 116(1) (1994) 54-57.

[40] Garcia A., Solano J.P., Vicente P.G, Viedma A., Flow pattern assessment in tubes with wire coil inserts in laminar and transition regimes, International Journal of Heat and Fluid Flow, 28 (2007) 516-525.

[41] Seban R.A., Mclaughin E.F., Heat transfer in tubes coils with laminar and turbulent flow, International Journal of Heat and Mass Transfer, 6 (1963) 387-395.

a)

b)

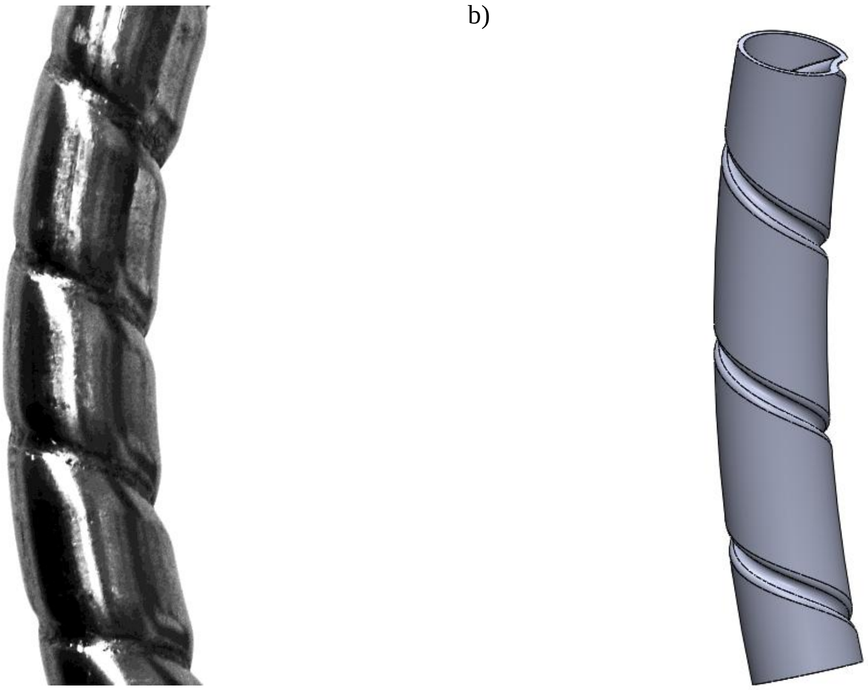

**Figure 1:** Picture (a) and sketch (b) of the corrugated wall coiled tube under test.

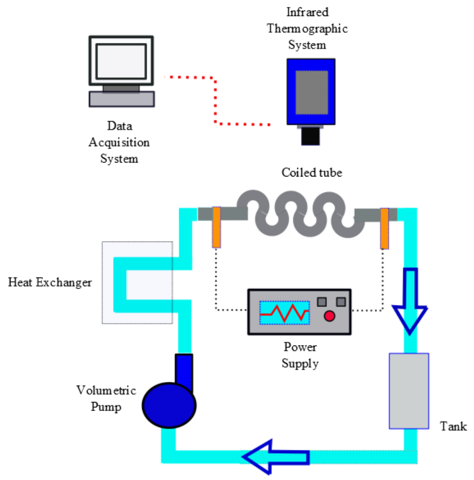


**Figure 2a:** Sketch of the experimental setup.

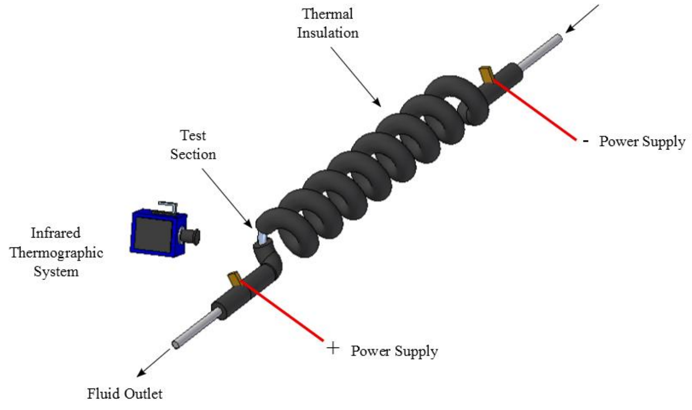


**Figure 2b:** Sketch of the infrared thermographic system arrangement.

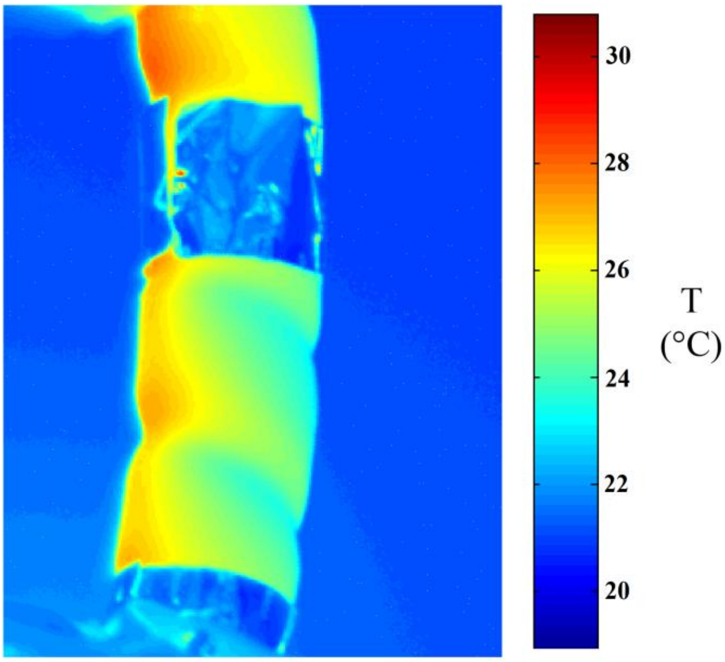


**Figure 3:** Representative infrared image.

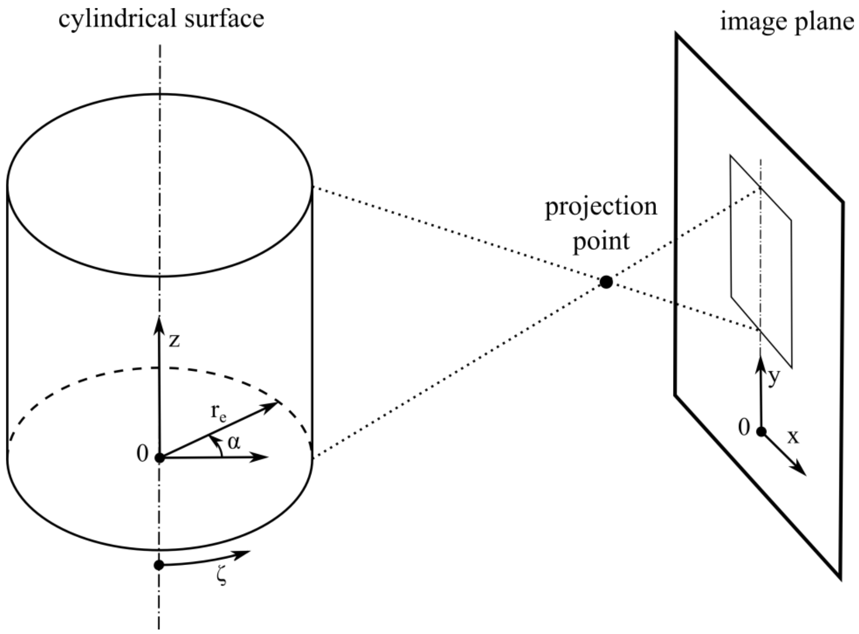


**Figure 4:** Cylindrical shape effect on the acquired image.

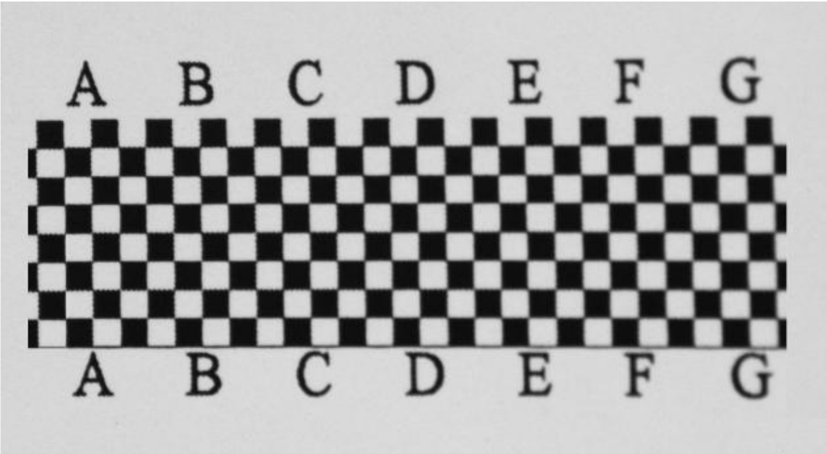


**Figure 5:** Input image.

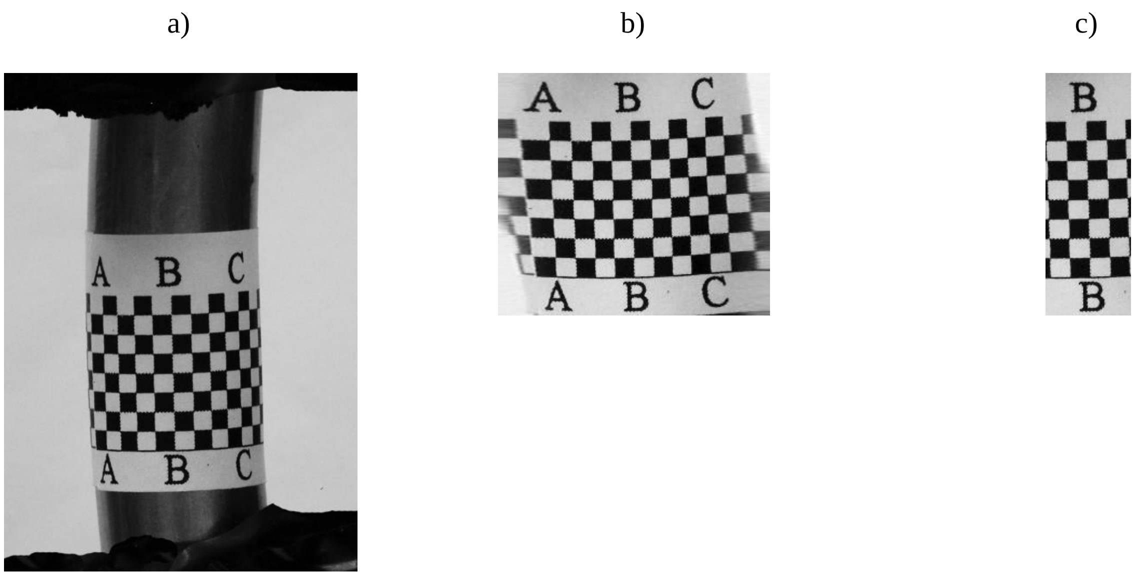


**Figure 6:** Image processing steps: a) input image; b) unwrapped image; c) cropped image.

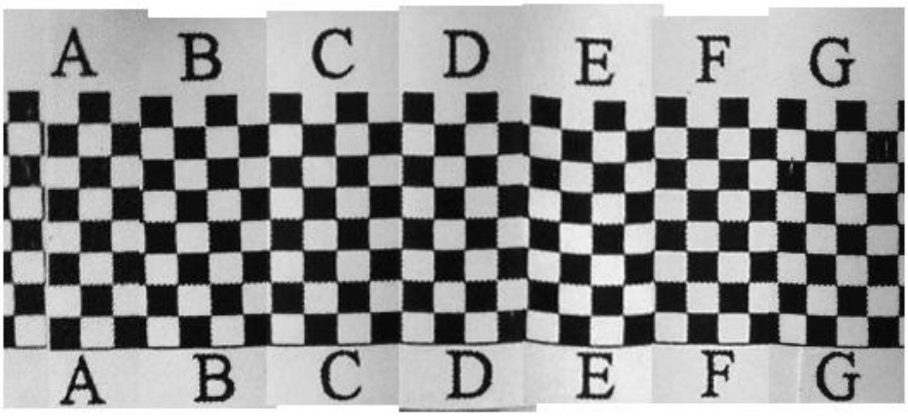


**Figure 7:** Unwrapped total image.

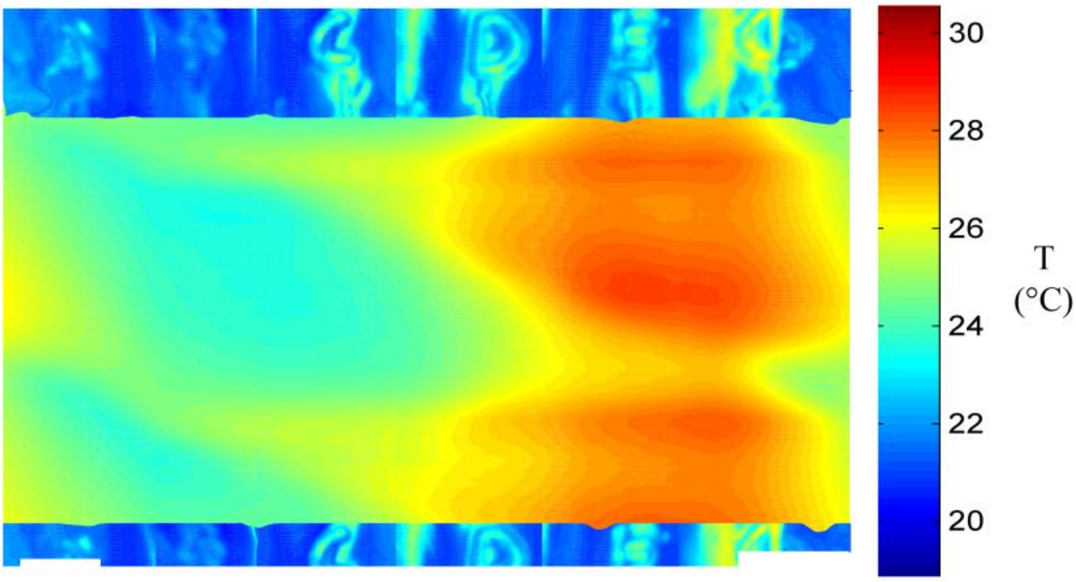


**Figure 8:** Unwrapped infrared image.

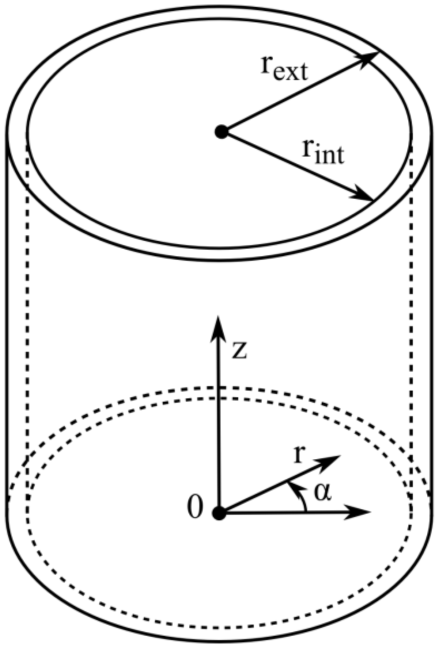


**Figure 9:** Simplified geometrical domain with coordinate system.

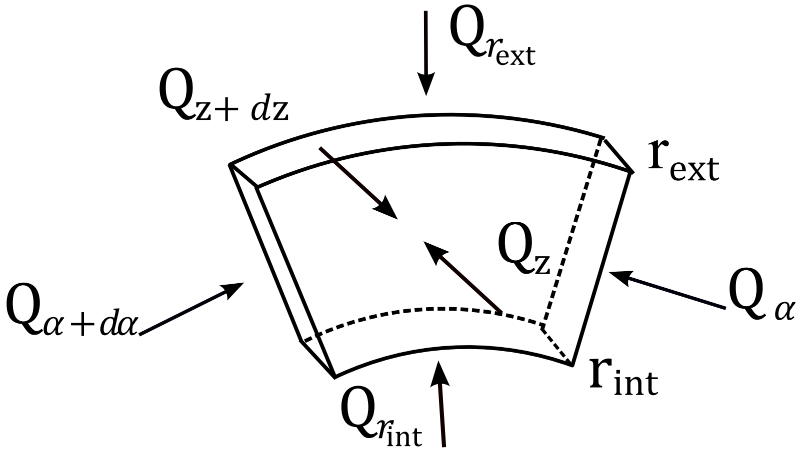


**Figure 10:** A portion of the test section.

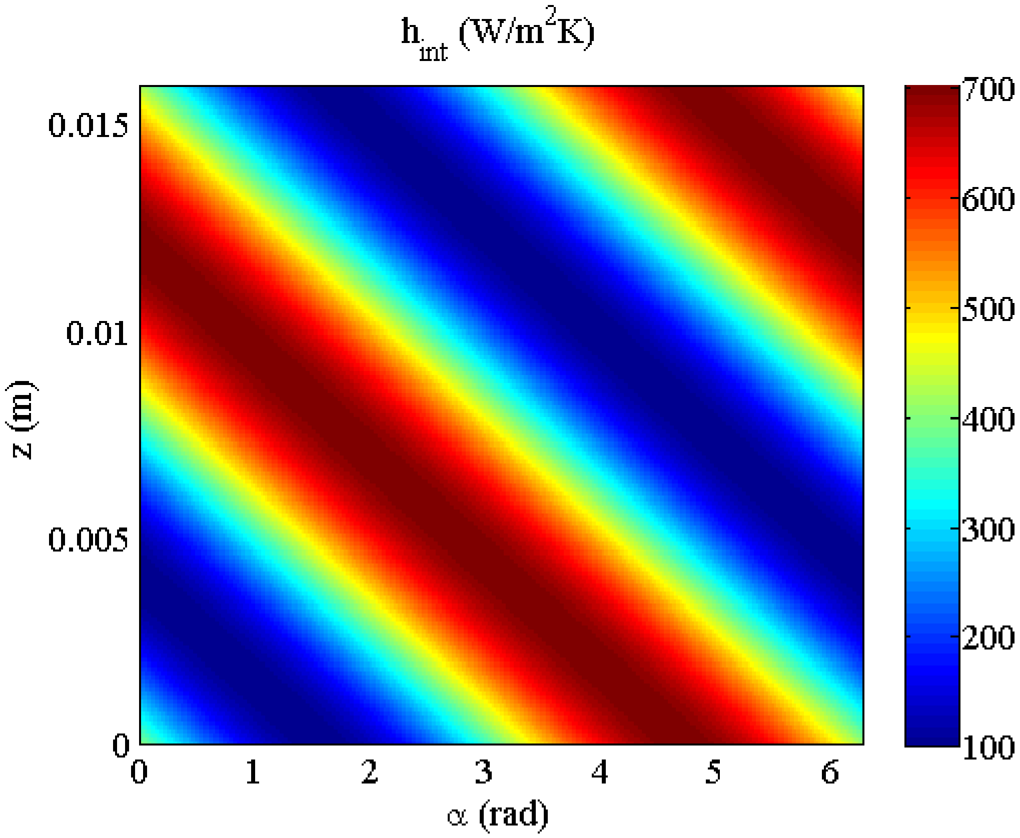


**Figure 11:** Distribution of $h_{int}$ adopted in the validation procedure.

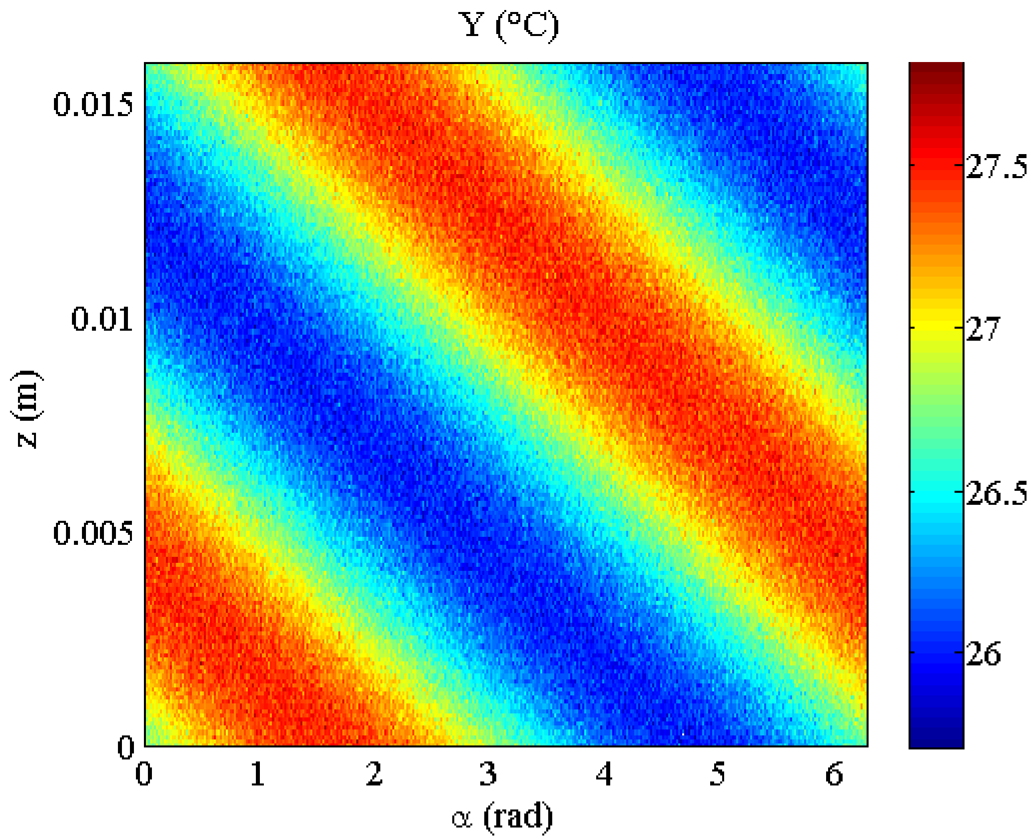


**Figure 12:** Synthetic temperature distribution on the external wall surface for the case with noise level $\sigma = 0.1$ K.

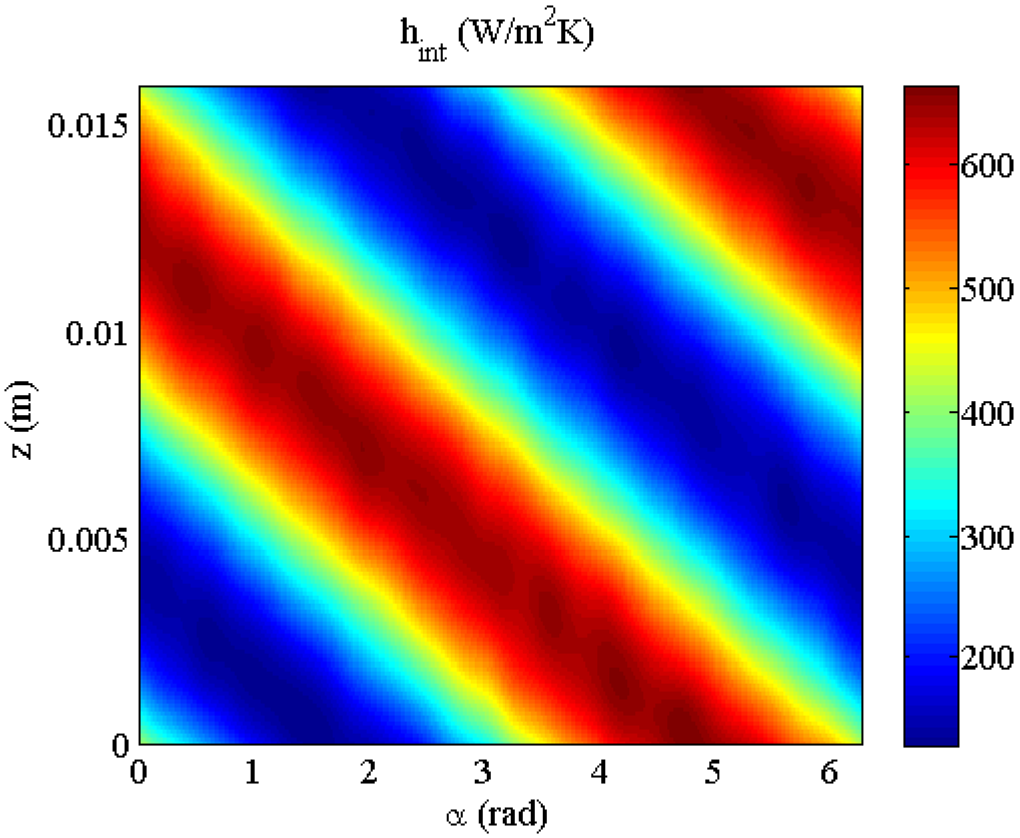


**Figure 13:** Restored distribution of the local convective heat transfer coefficient $h_{int}$ for the case with noise level
$\sigma = 0.1$ K.

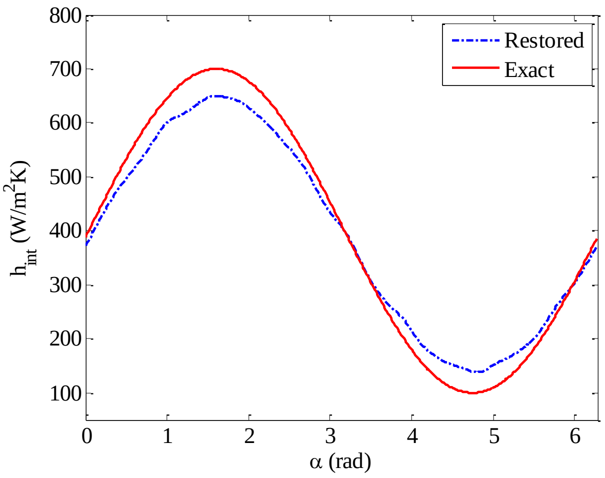


**Figure 14a:** Exact and restored $h_{int}$ along the circumferential coordinate at z=0.08 m for the case with noise level σ = 0.1 K.

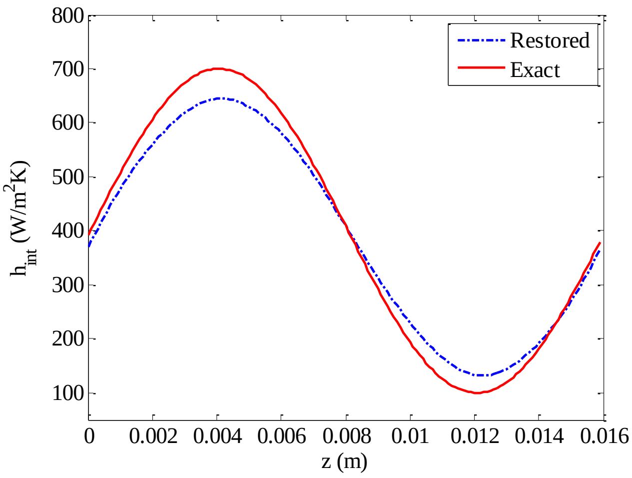


**Figure 14b:** Exact and restored $h_{int}$ along the axial coordinate at α=0 rad obtained by applying Gaussian Filter Technique for the case with noise level σ = 0.1 K and $u_c$ = 0.13 rad$^{-1}$.

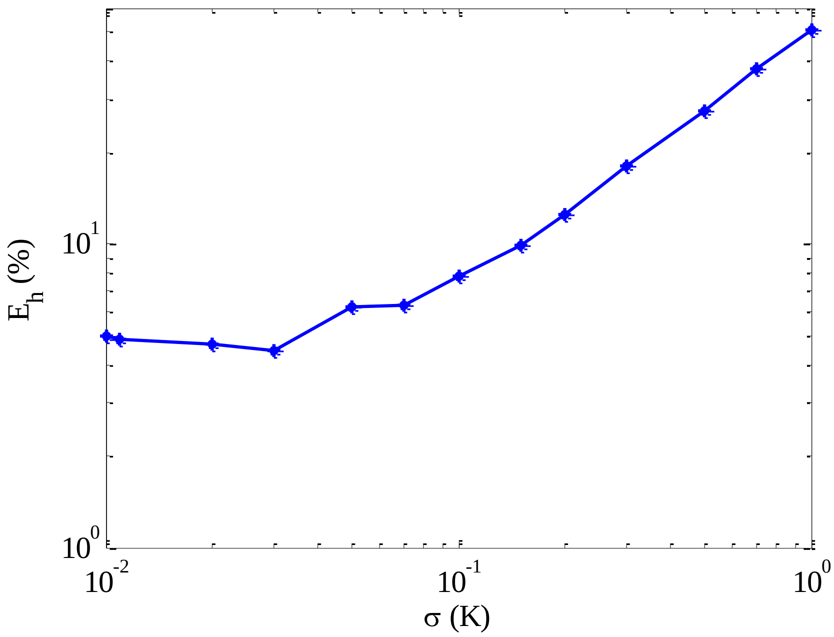


**Figure 15:** Estimation error on $h_{int}$.

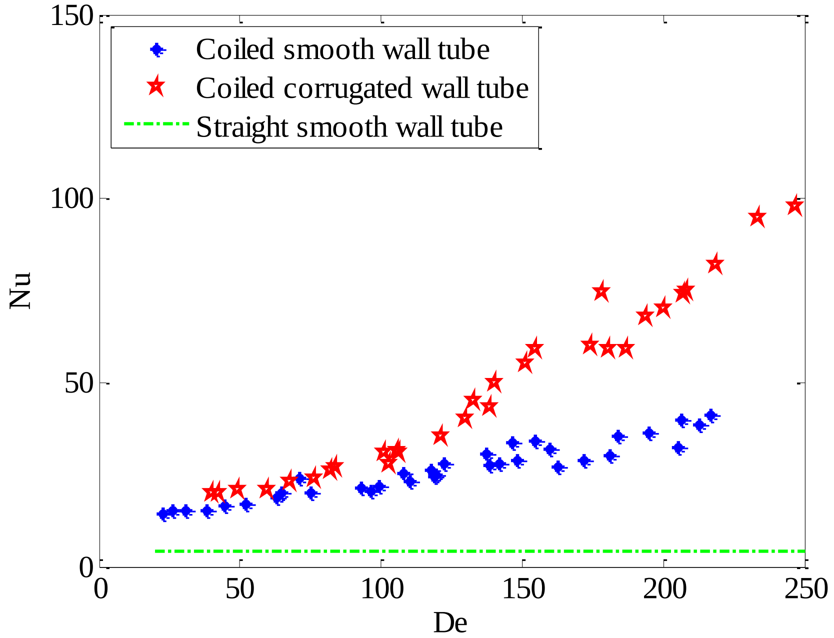


**Figure 16**: Asymptotic Nusselt number vs De for the helically coiled tubes under test and comparison with the straight smooth tube analytical solution [35].

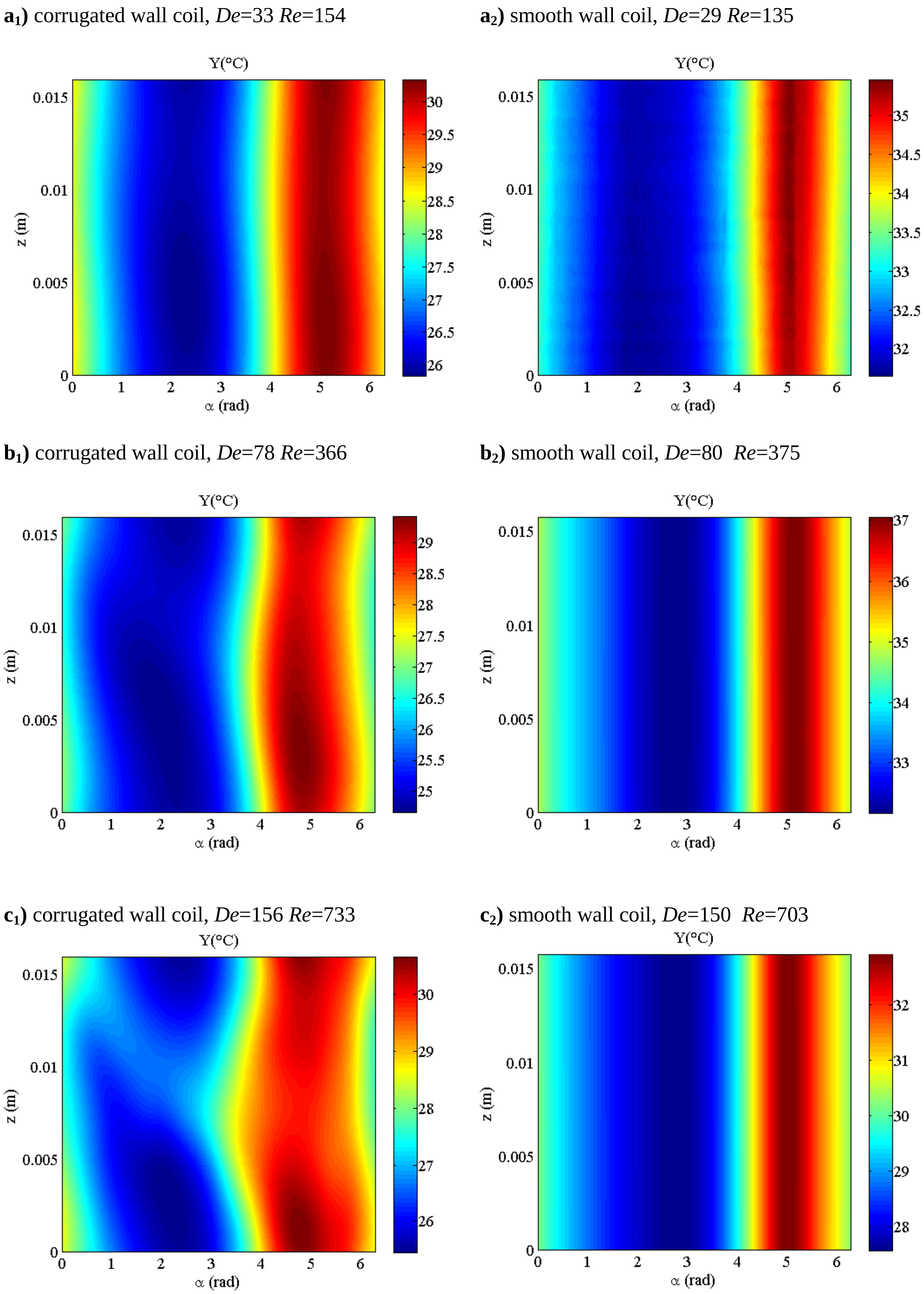
a1) corrugated wall coil, De=33 Re=154
a2) smooth wall coil, De=29 Re=135
b1) corrugated wall coil, De=78 Re=366
b2) smooth wall coil, De=80 Re=375
c1) corrugated wall coil, De=156 Re=733
c2) smooth wall coil, De=150 Re=703
Y(°C)
z (m)
α (rad)
0.015
0.01
0.005
0
0 1 2 3 4 5 6

**$d_1$)** corrugated wall coil, *De*=207 *Re*=975 **$d_2$)** smooth wall coil, *De*=215 *Re*=1006

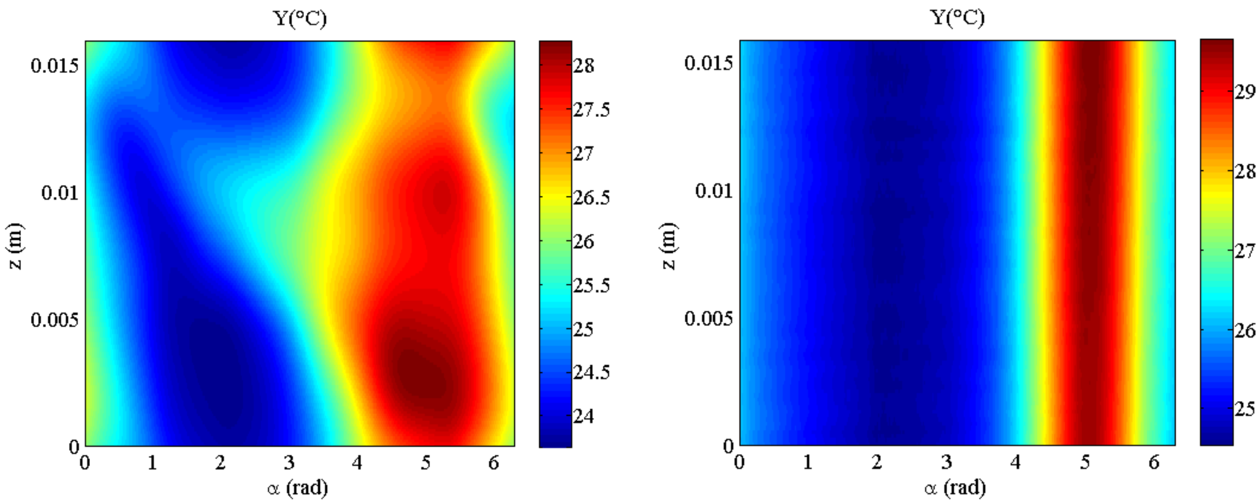


**Figure 17:** Wall temperature distribution for the corrugated and smooth wall coiled tubes.

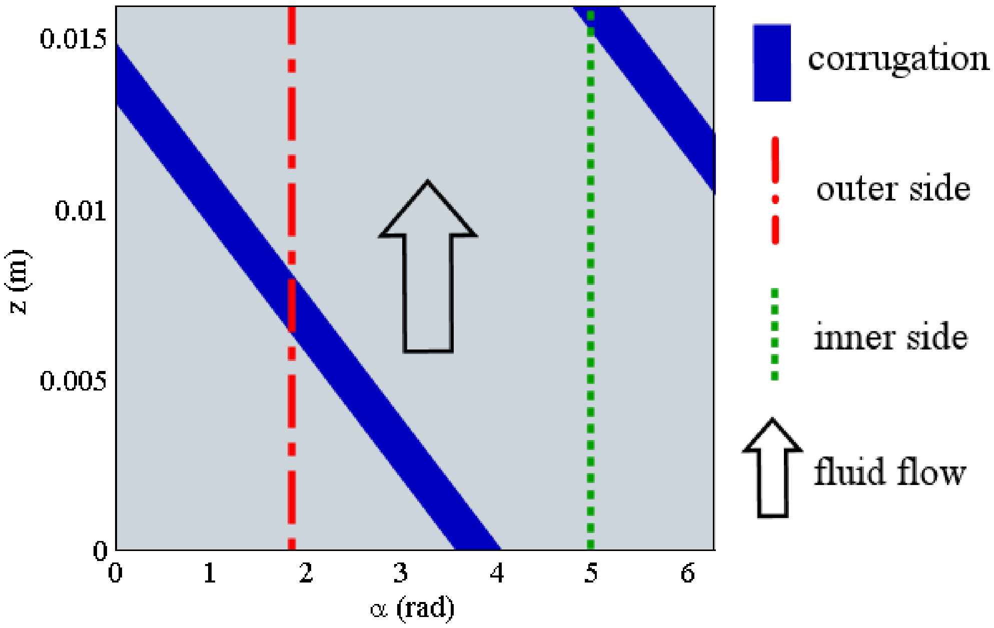

**Figure 18:** Wall corrugation, outer and inner side of the coil on test section surface.

**a₁)** corrugated wall coil, *De*=33 *Re*=154

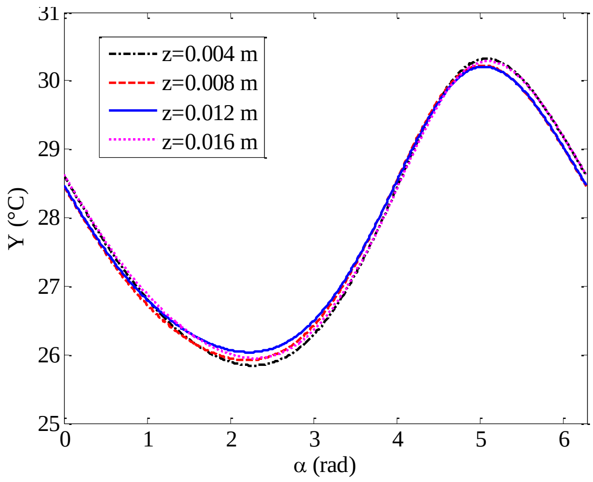


**a₂)** smooth wall coil, *De*=29 *Re*=135

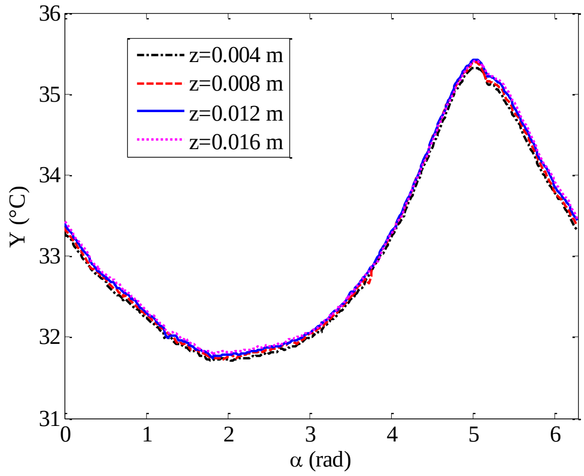


**b₁)** corrugated wall coil, *De*=78 *Re*=366

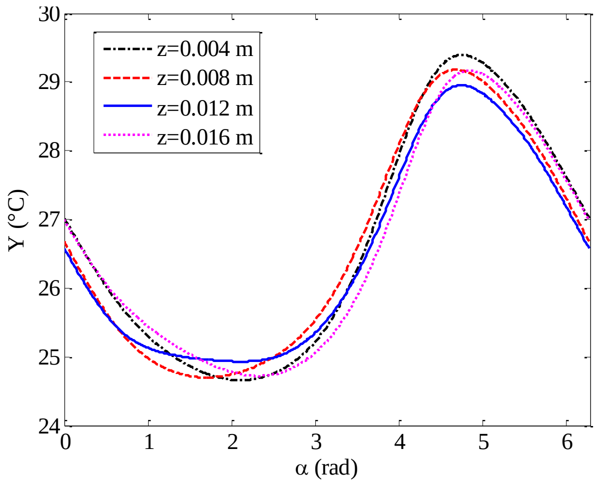


**b₂)** smooth wall coil, *De*=80 *Re*=375

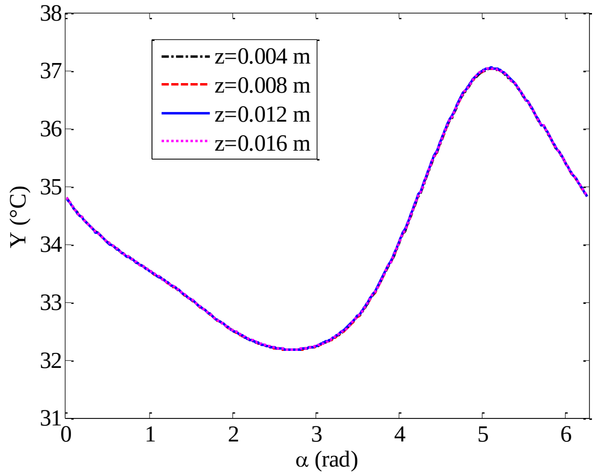


**c1)** corrugated wall coil, *De*=156 *Re*=733

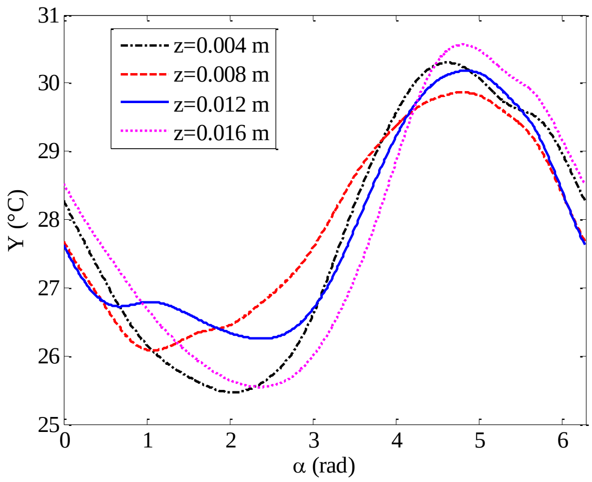


c₂) smooth wall coil, *De*=150 *Re*=703

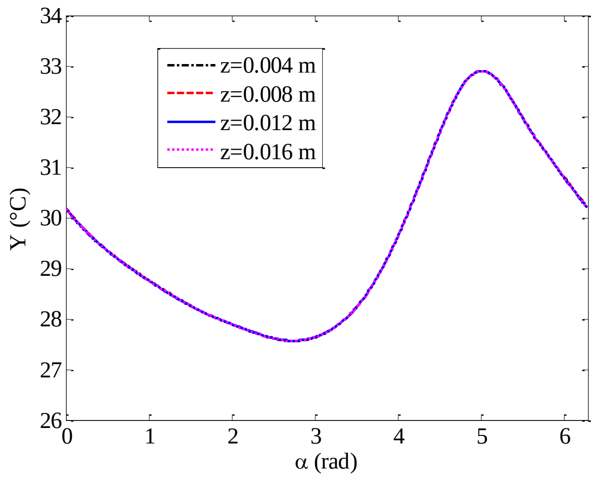

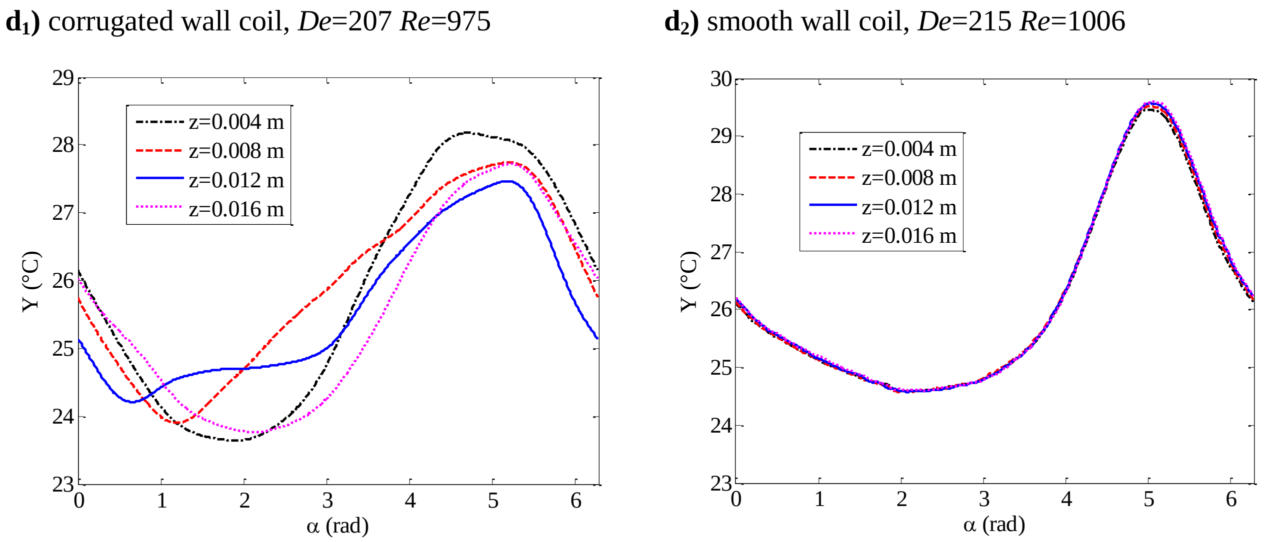


**Figure 19:** Circumferential temperature distribution at different axial location for the corrugated and smooth wall coiled tubes.

**a$_1$)** corrugated wall coil, *De*=33 *Re*=154

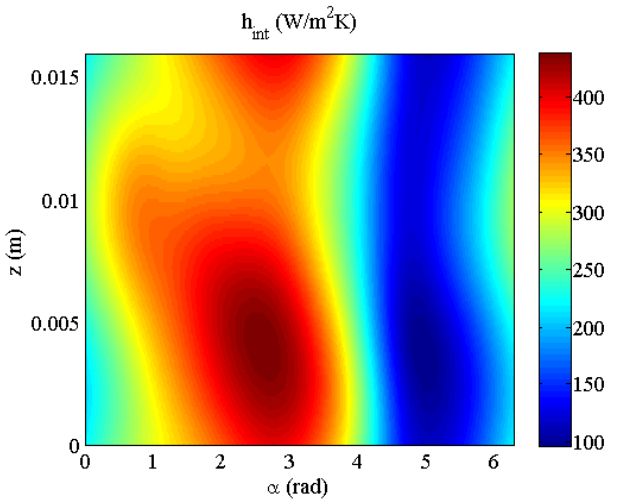


**a$_2$)** smooth wall coil, *De*=29 *Re*=135

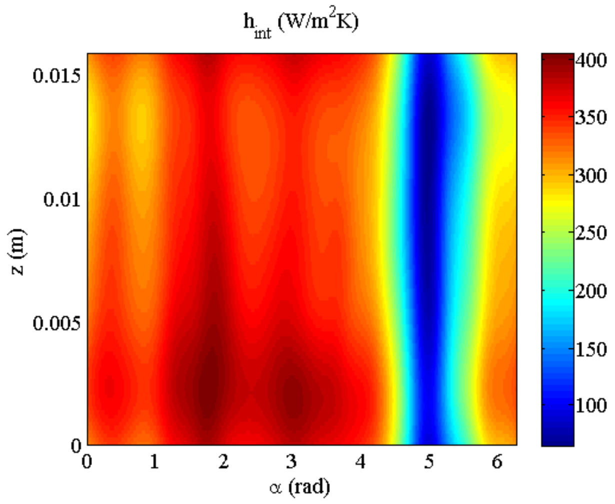


**b$_1$)** corrugated wall coil, *De*=78 *Re*=366

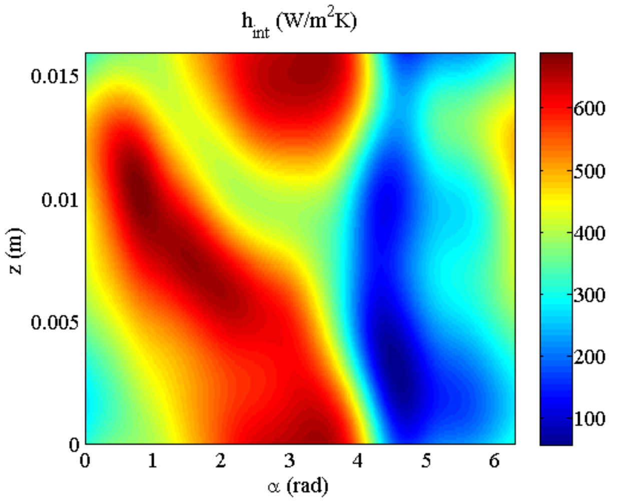


**b$_2$)** smooth wall coil, *De*=80 *Re*=375

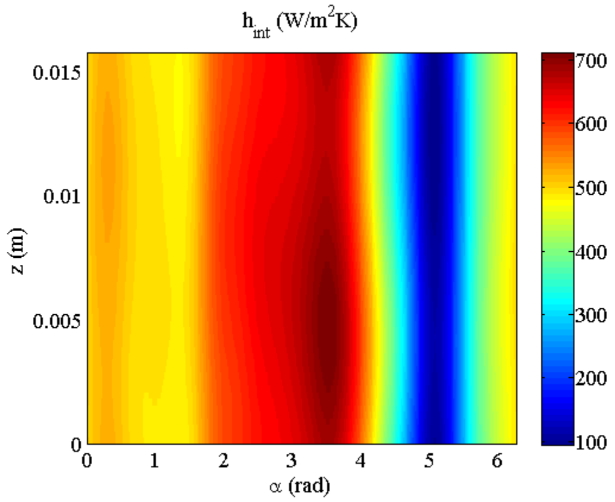


**c1)** corrugated wall coil, *De*=156 *Re*=733

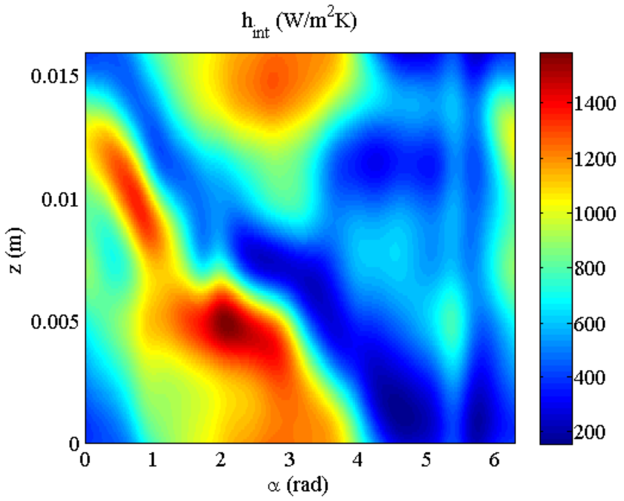


**c$_2$)** smooth wall coil, *De*=150 *Re*=703

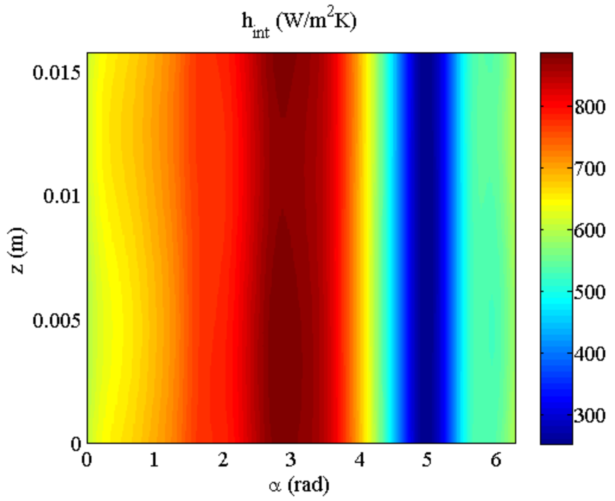

**d$_1$)** corrugated wall coil, *De*=207 *Re*=975 **d$_2$)** smooth wall coil, *De*=215 *Re*=1006

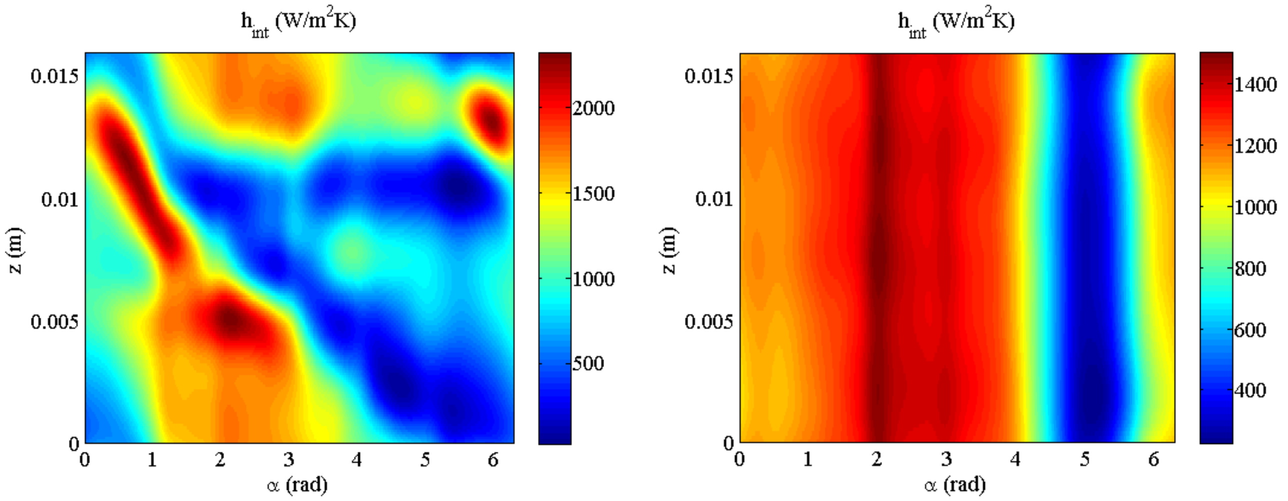


**Figure 20:** Convective heat transfer coefficient distribution for the corrugated and smooth wall coiled tubes.

**a₁)** corrugated wall coil, *De*=33 *Re*=154

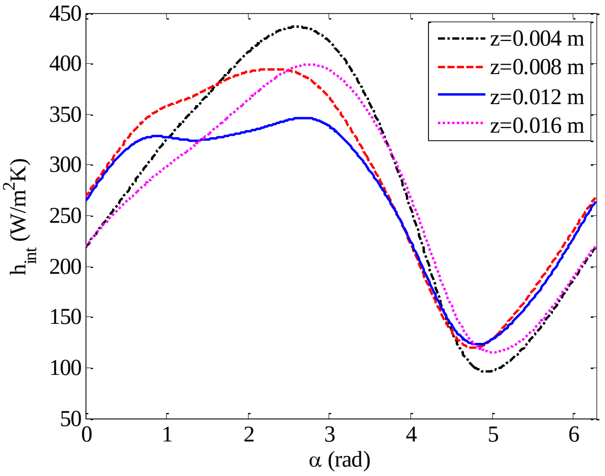


**a₂)** smooth wall coil, *De*=29 *Re*=135

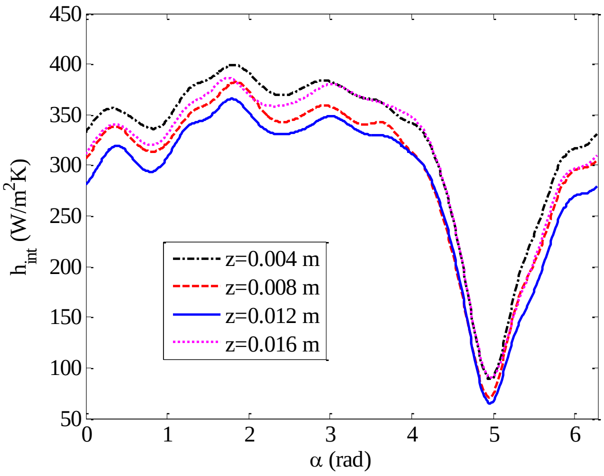


**b₁)** corrugated wall coil, *De*=78 *Re*=366

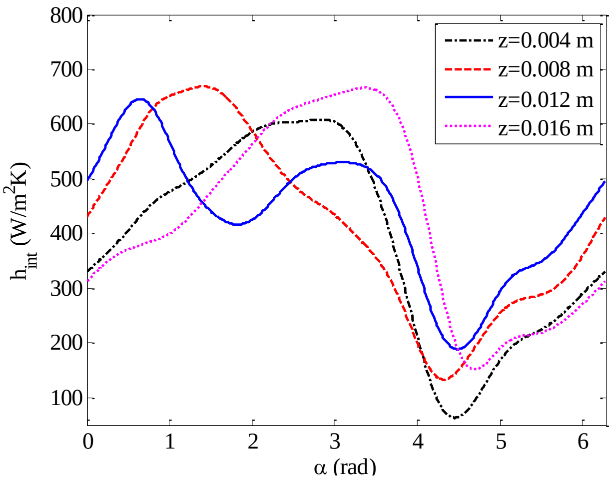


**b₂)** smooth wall coil, *De*=80 *Re*=375

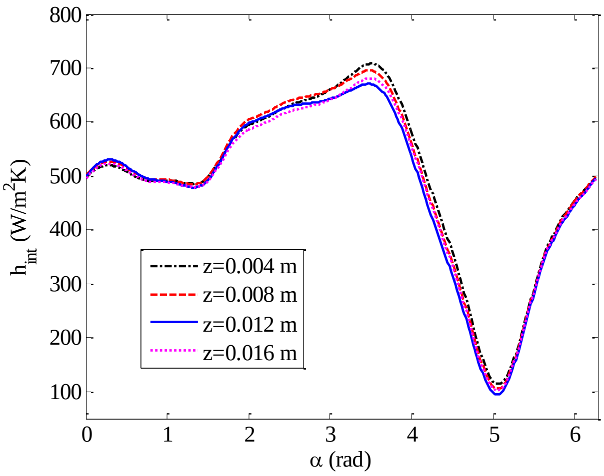


**c1)** corrugated wall coil, *De*=156 *Re*=733

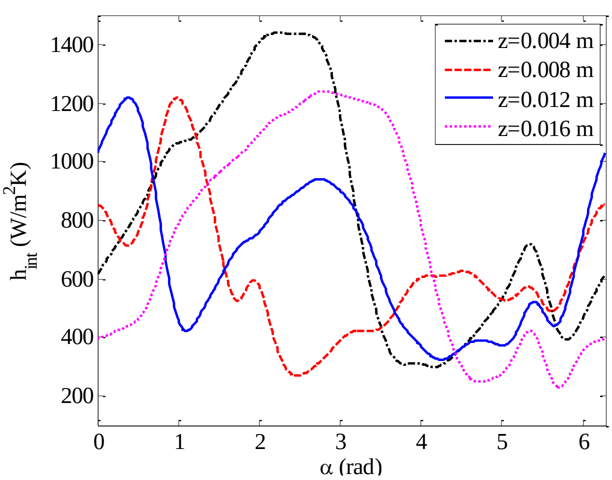


**c₂)** smooth wall coil, *De*=150 *Re*=703

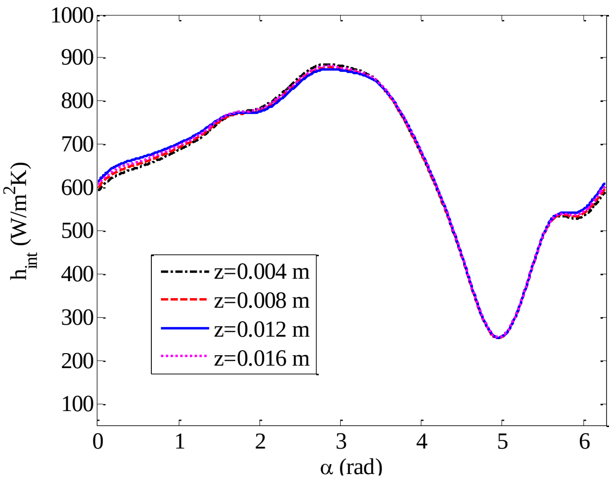

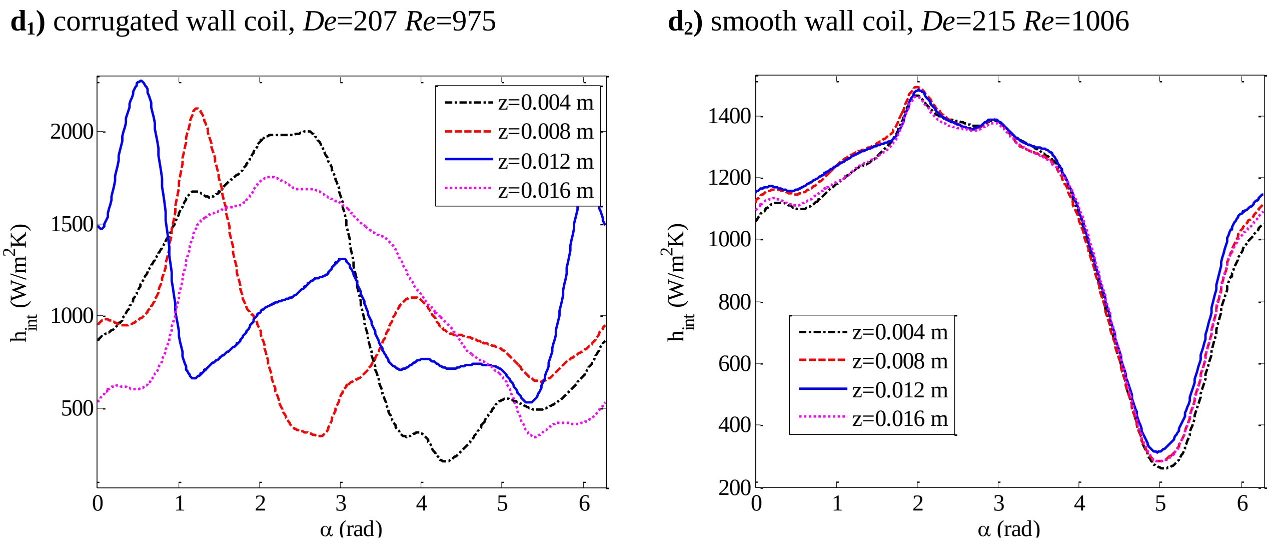


**Figure 21:** circumferential convective heat transfer coefficient distribution at different axial location for the corrugated and smooth wall coiled tube.

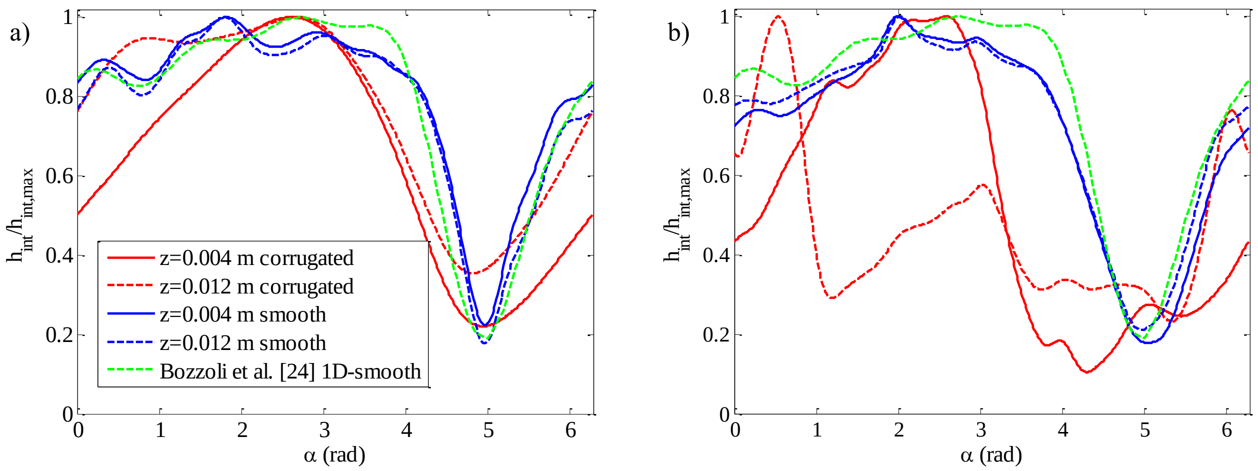


**Figure 22:** Normalized local convective heat transfer coefficient for *De*≅ 30 (a), *De*≅ 210 (b) and comparison with the data for smooth wall coils by Bozzoli et al. [24]